Structural Performance of Early 20th Century Masonry High Rise Buildings

by

Rebecca Buntrock

Bachelor of Engineering, Civil Engineering and Applied Mechanics
McGill University, 2007

Submitted to the Department of Civil and Environmental Engineering
In Partial Fulfillment of the Requirements of the Degree of

MASTER OF ENGINEERING
in Civil and Environmental Engineering
at the

MASSACHUSETTS INSTITUTE OF TECHNOLOGY

June 2010

Signature of the Author_____

Rebecca Buntrock
Department of Civil and Environmental Engineering
May 7, 2010

Certified by_____

John A. Ochsendorf
Associate Professor of Civil and Environmental Engineering and Architecture
Thesis Supervisor

Accepted by_____

Daniele Veneziano
Chairman, Departmental Committee for Graduate Students

Structural Performance of Early 20th Century Masonry High Rise Buildings

by

Rebecca Buntrock

Submitted to the Department of Civil and Environmental Engineering
On May 7, 2010 in Partial Fulfillment of the
Requirements of the Degree of Master of Engineering in
Civil and Environmental Engineering

ABSTRACT

Early generation high rise buildings built between 1890 and World War II represent a technical transition between traditional load bearing masonry construction and modern curtain wall systems, and are typically referred to as 'transitional masonry buildings'. These structures comprise a large percentage of the building stock constructed in the early twentieth century. Two pertinent issues have emerged with these structures as they age. The first is the deterioration of the exterior masonry façade, which is largely a result of deficiencies in the construction method of these structures. The second issue is that it is very difficult to properly predict their structural performance because of the complicated interaction between the masonry infill and the structural frame. Underestimating or misdiagnosing the structural performance of a transitional masonry building can result in improper interventions. The aim of this thesis is to increase the understanding of the structural and façade performance of transitional masonry buildings and present methods for their analysis. A case study of a transitional masonry building is structurally analyzed using linear and nonlinear procedures to determine the contribution of the masonry infill as well as to investigate the feasibility of using simplified analytical models to predict structural performance.

Thesis Supervisor: John A. Ochsendorf
Title: Associate Professor of Civil and Environmental Engineering and Architecture

Acknowledgement

The publication of this thesis would not have been possible without the help and support of many people, all of whom deserve my thanks and appreciation.

Firstly, sincere thanks to my advisor, Professor John Oschendorf, for his helpful guidance during the research and writing of this paper. It was a great opportunity to work with someone with his experience and dedication to the field of structural analysis of historic construction.

I also wish to thank Professor Jerome Connor for providing leadership and guidance throughout this program, in particular for all the enjoyable classes he taught. Thank you also to teaching assistant Simon Laflamme for his help during this program.

Thank you to the firm Gale Associates for their helpful support throughout this year, both financially and personally.

Thank you to my friend and colleague Olga Hathaway, both for her advice during the writing of this paper, and also for introducing me to the field of historic preservation.

Thank you to all the friends I have been lucky enough to make in the M.Eng program for making this year so enjoyable and memorable.

Finally, I would like to thank my parents Barbara and Ken, my brother Mark, and my friend Jeanne for their continuous support and encouragement.

Table of Contents

APPENDICES

List of Figures

List of Tables

All photographs without citation are from the author and the firm Gale Associates.

1. Introduction

In the late nineteenth century, the introduction of the skeletal-steel frame in building construction changed the way that structures were built. It allowed designers to build much higher without the constraints of large wall thicknesses at a structure's base, which brought about a period of construction combining new and old building techniques. Built between 1890 and World War II, these early generation high rise buildings were constructed with the steel frame encased in massive masonry walls. They represent a technical transition between traditional load bearing masonry construction and modern curtain wall systems, and are typically referred to as 'transitional masonry buildings'. These structures comprise a large percentage of the building stock constructed in the early twentieth century.

Two pertinent issues have emerged with these structures as they age. The first is the deterioration of the exterior masonry façade, which is largely a result of deficiencies in the construction method of these structures. The second issue is that it is very difficult to properly predict their structural performance because of the complicated interaction between the masonry infill and the structural frame. The ability to assess the performance and strength of these structures is important for making proper retrofit decisions.

1.1 Assessment of Transitional Masonry Structures

What makes transitional masonry structures so unique when compared to other eras of construction? Firstly, the detailing of these structures did not accommodate for differential movement of the various materials in the wall assembly, not did it provide adequate corrosion protection of the embedded steel frame. The interaction between the steel frame and masonry infill under structural movement has resulted in specific patterns of façade deterioration.

Secondly, the combination of having both a skeletal-steel frame as well as solid masonry walls makes transitional masonry buildings highly indeterminate from a structural analysis perspective. Under lateral loading, the structure and masonry wall will interact under one of many different potential failure mechanisms, each which alter the total resistance of the structure differently. Masonry is discontinuous, anisotropic, and brittle by nature, and its behavior is very difficult to accurately predict using numerical models. A consensus on a realistic yet simple analytical model to predict the contribution of masonry infill does not exist, making it difficult to identify the lateral load resistance of these buildings.

The aforementioned issues make the renovation of transitional masonry buildings a challenging task, both from a building restoration and structural engineering perspective. When specifying façade repairs, applying traditional materials restoration techniques without addressing the underlying cause of deterioration will be at best a temporary fix. Furthermore, introducing additional elements to the wall assembly, such as thermal insulation, has the potential to negatively affect the dynamics of the wall assembly and further accelerate corrosion. Structurally, neglecting the contribution of the masonry infill to the lateral load performance will result in inaccurate predictions of strength, stiffness, and failure mechanisms of the building. Underestimating or misdiagnosing the structural performance of a transitional masonry building can result in unnecessary or improper interventions.

1.2 Research Motivation and Objectives

The aim of this thesis is to increase the understanding of the structural and façade performance of transitional masonry buildings and present methods for their analysis. The following points provide the general motivation for this work.

- When restoring transitional masonry façades, mechanisms of deterioration resulting from the interaction between the masonry infill and structural frame must be understood in order to properly specify repairs, renovations, or energy upgrades.
- It is necessary to account for the structural contribution of the masonry infill when evaluating transitional masonry buildings in order to properly predict behavior under lateral loads.

To meet this objective, this thesis begins by providing a classification of transitional masonry wall systems, their mechanisms of deterioration, and the existing methods available for their structural analysis. A case study of transitional masonry building is then structurally analyzed using linear and nonlinear procedures to determine the contribution of the masonry infill as well as to investigate the feasibility of using simplified analytical models to predict structural performance. The feasibility of performing an energy upgrade on a transitional masonry building is then explored. The thesis concludes by presenting procedures for the evaluation of an existing transitional masonry building, issues to consider when specifying façade repairs, and structural retrofit options.

2. Classification of Transitional Masonry Wall Systems

Early generation transitional high rise structures have been exposed to the built environment for over a century and in many cases have begun to require significant repair. Their unique method of construction has resulted in specific patterns of façade deterioration, which is largely a result of interaction between the masonry curtain wall and embedded steel frame. Exterior defects resemble those typically found in traditional unreinforced masonry (URM) bearing wall construction, such as cracked brick and displaced masonry, but unlike traditional construction, the causes of defects in transitional masonry buildings are largely structural in nature (Friedman, 2005). Since the majority of these structural steel members are embedded within thick masonry walls, information on the deterioration level of transitional masonry structures can only be fully verified through destructive testing. However, because the patterns of façade deterioration correlate to specific structural issues, they can be a helpful indication of the condition of the underlying structural frame.

This Chapter begins by classifying transitional masonry wall systems compared to earlier (bearing wall) and later (modern curtain wall) systems. The different modes of façade deterioration and how they are related to the building construction are then presented in detail.

2.1 Bearing Wall Construction

Prior to the advent of steel frame construction in the late nineteenth century, most tall buildings were constructed with load bearing URM walls that supported their own weight as well as portions of the building's floor and roof load. Masonry bearing walls were not engineered but designed empirically based on tables published in local building laws. These laws specified wall thickness as a function of the building height to keep the maximum compressive stress in the masonry below allowable values, which included very conservative factors of safety. Structural height was limited by the low tensile capacity of the brick masonry and the impracticality of large wall thicknesses required at the base of the structure. The tallest high rise structure in North America supported by solid load bearing walls is the 16-story Monadnock Building (1891) in Chicago, which has walls that are six feet thick at its base (O'Brien, 2006).

Historically, masonry bearing walls were not designed for wind loads despite the fact that they are the main force resisting system under lateral loads. In most cases, the large axial compressive stress in the wall due to self weight compensates for wind-induced bending stresses, maintaining ideal compression-only conditions across the wall's section. Floor systems were commonly flexible diaphragms constructed

of heavy timber joists and wood decking, which deflect along with the bearing wall as it settles or moves. As there are no other elements with comparable lateral stiffness to the bearing walls, these structures tend to move uniformly, negating the need for expansion joints required in modern multi-layered walls. Introducing discontinuities or joints in the bearing walls in fact undermines structural integrity of the system (Friedman and Oppenheimer, 1997). As such, bearing wall construction also incorporates relatively conservative wall to window ratios because it was not advantageous to cut holes into the primary structural system.

In addition to their structural role, multi-wythe masonry walls in traditional construction act as the primary controller of air, water, and heat transfer from the exterior to interior of the structure. These structures rely on the mass of the masonry for temperature and moisture control. The intent of this type of wall system is to absorb water naturally and disperse it through evaporation to either the interior or the exterior of the building during summer or winter conditions respectively.

2.2 Transitional Masonry Wall Construction

By the early twentieth century, the skeletal-steel frame emerged as the dominant structural form for building construction, replacing previous methods such as bearing wall systems. Structural steel had become the preferred metal for use in building construction over wrought and cast iron due to its ability to provide stiffer riveted connections and superior lateral resistance (Leslie, 2009). High rise structures were detailed to have solid masonry exterior walls built integrally around the steel frame, representing a hybrid system that combined characteristics of load bearing masonry and modern curtain walls. In most structures built during this time period, the multi-wythe masonry curtain walls ("infill") are supported by spandrel beams at each floor level. They were intended to carry no building loads aside from their own self weight and localized wind loading (Kidder, 1906). This allowed for a reduction in masonry wall thickness required by building laws, as shown in Figure 1. Note that during this time period, transitional masonry façades were referred to as curtain walls, although they are distinctly different from modern curtain walls. Skeletal-steel framing provided increased flexibility in construction sequencing because exterior walls no longer had to be constructed from the ground-up. This framing system permitted building heights much taller than had previously been achieved, thus beginning the skyscraper era of the early 1900s (Friedman, 1995).

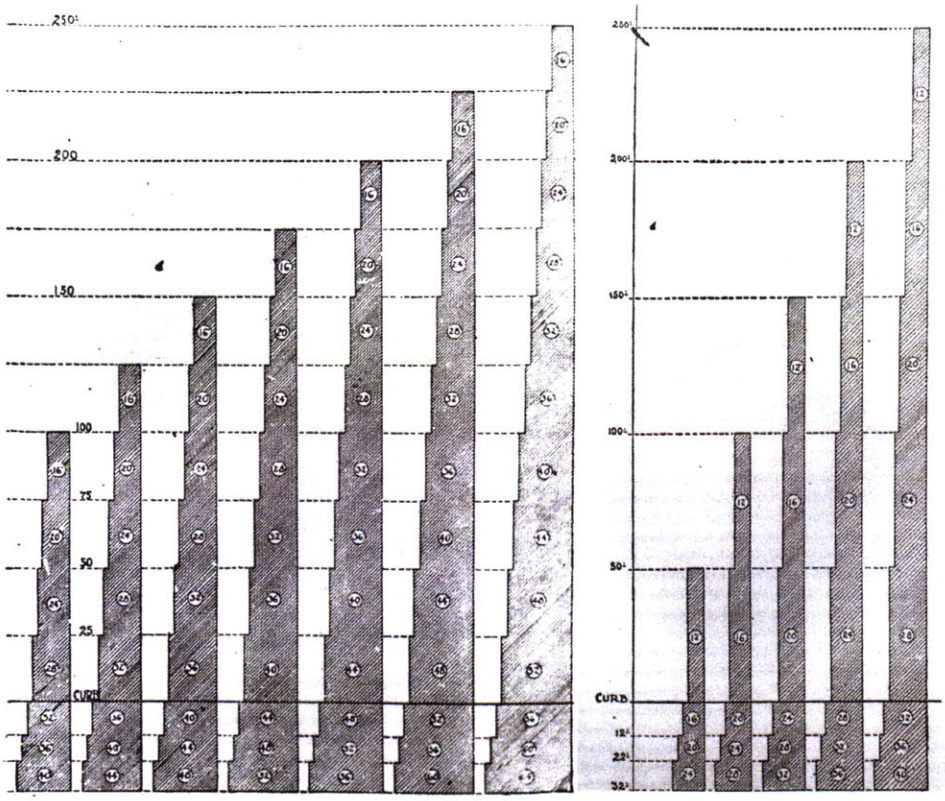

Figure 1: Thickness Specifications of Bearing Walls (left) and Transitional Masonry Walls (right)
Source: Birkmire, 1906

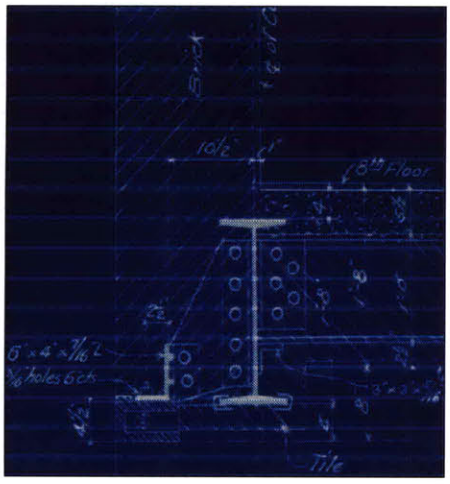

Figure 2: Shelf Angle and Spandrel Beam
Source: Boston Public Library, 1912

Façades in transitional masonry structures typically have an outer wythe of high quality face brick, stone ashlar, or decorative terra-cotta veneer, often in combination, in front of multiple wythes of common brick or terra-cotta back-up held together by a lime-based mortar. Metal anchors or masonry headers connect the outer wythe of masonry to the masonry back-up to achieve a composite wall system. The outer wythe of masonry is usually intermediately supported at each floor level by shelf angles or outriggers connected to spandrel beams (shown in Figure 2), although in some cases it is only supported at grade (Searls and Bronski, 2000). Curtain wall architectural graphic standards from this time period are shown in Figure 3.

The primary intended function of the exterior wall system was non-structural in nature. It was to provide fireproofing and protection against the elements for the metal-work (Birkmire, 1906). This

would prove to be problematic for long-term performance of the embedded building components. Structural steel members were sometimes coated with a layer of oil, tar, red lead paint, cement, or a sheet of asphaltic felt to prevent oxidation, but the main reliance for corrosion protection was placed on the natural alkalinity of the infill mortar surrounding the frame elements (Birkmire, 1906). The steel columns are encased in fire-proofing brick masonry piers along the building's height, which ties them directly to the rigid masonry walls. Although building handbooks cautioned architects that "[they] should not lose sight of expansion and contraction due to variations in temperature" when combining masonry and steel, there were no provisions for horizontal or vertical expansion joints to allow for differential movement (Twelvetrees, 1900, pg 232).

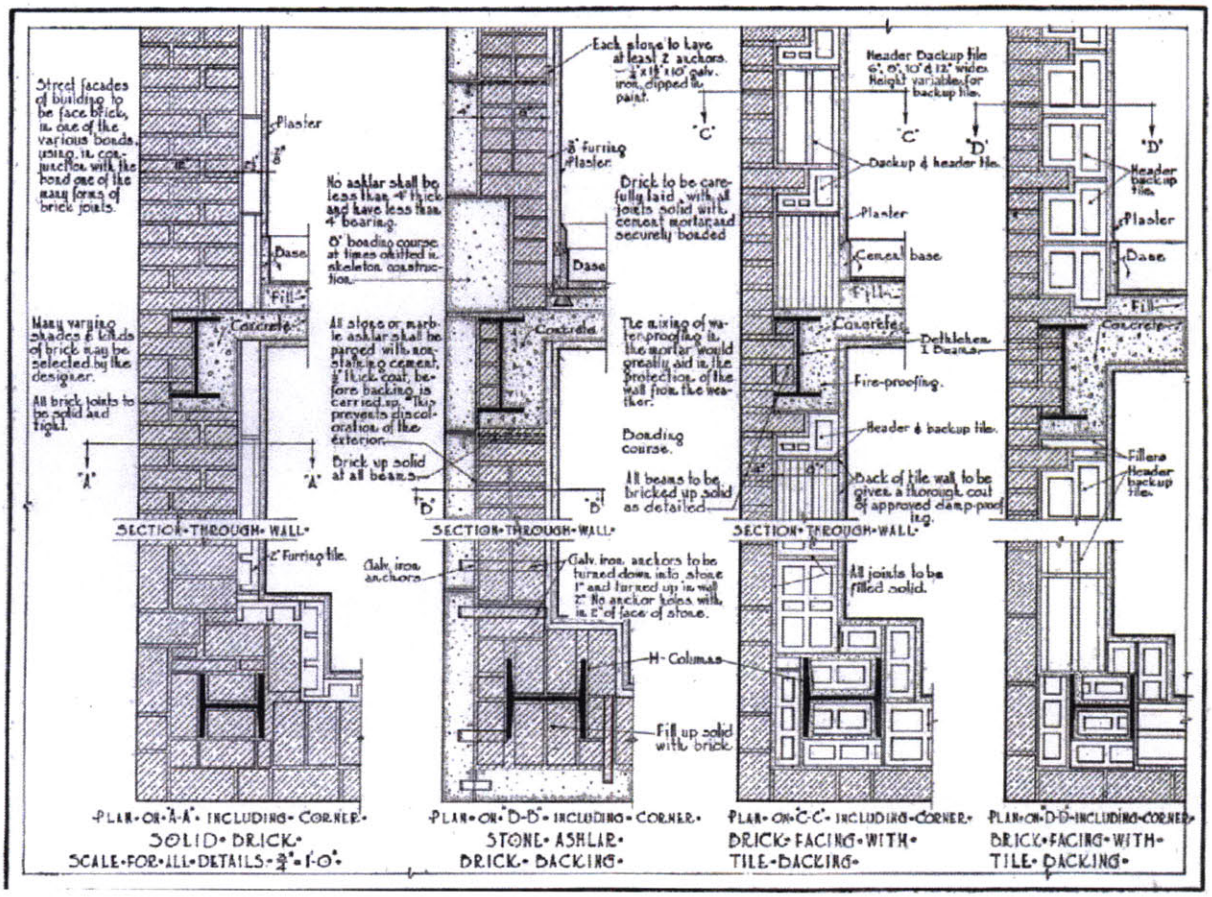

Figure 3: Curtain Wall Details
Source: Knobloch, 1931

Floor systems in transitional high rise structures are typically rigid terra-cotta tile arches or an archaic form of reinforced concrete slabs (Friedman, 1995). Connections in skeletal steel frames were commonly riveted until the modern shear connection was introduced after World War II (Rabun, 2000). Column to girder connections are top and bottom clip angles or tees riveted to member flanges. For

structures with relatively low height-to-width ratios, these semi-rigid moment connections were intended to provide the primary lateral load support, although in reality the massively stiff masonry walls were absorbing the wind loads. Building construction experts during this time period asserted that a wind pressure of 30 pounds per square foot (psf) should be used in the design of high rise steel frames and it was generally safe to neglect wind pressures from buildings ten stories or less where the average width is not less than one-third the height (Kidder, 1921). No seismic provisions are mentioned in historic building codes prior to 1927, which was the first year seismic regulations were included as a voluntary appendix in the Uniform Building Code (Holmes, 2009). For taller structures, various different types of wind bracing were recommended, including gusset-plate, knee-brace, sway-rod, latticed girder, or portal type; these types of bracing are not described in detail in this text but are shown in Figure 4.

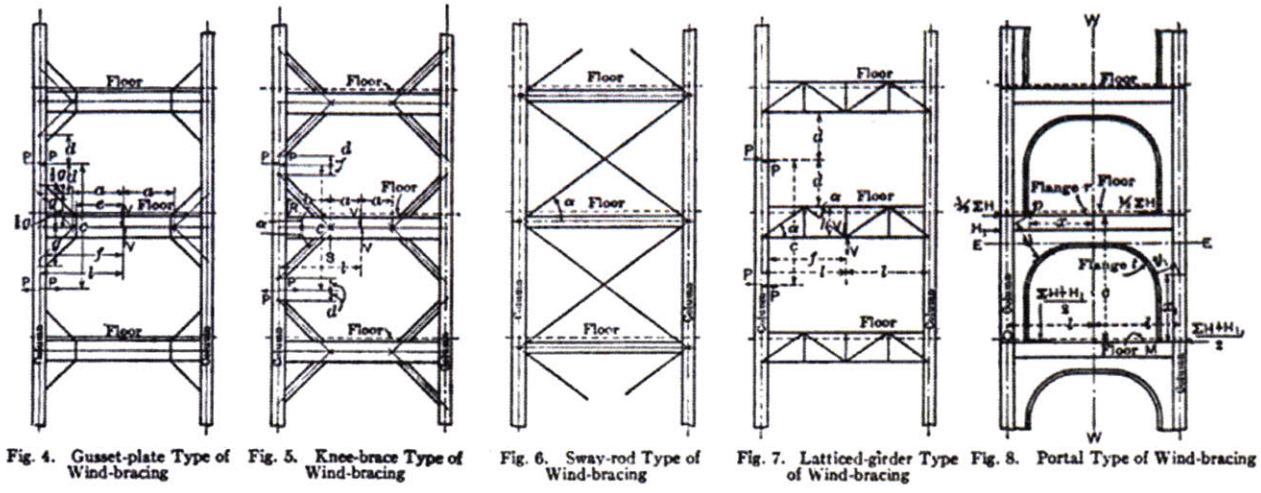

Fig. 4. Gusset-plate Type of Wind-bracing
Fig. 5. Knee-brace Type of Wind-bracing
Fig. 6. Sway-rod Type of Wind-bracing
Fig. 7. Latticed-girder Type of Wind-bracing
Fig. 8. Portal Type of Wind-bracing

Figure 4: Types of Recommended Wind Bracing for High Rise Structures
Source: Kidder, 1917

2.3 Problems with Transitional Masonry Façades

Modern understanding of building construction identifies deficiencies inherent in the detailing of transitional masonry façades, primarily the lack of accommodation for differential movement of materials and improper weatherproofing of the structural steel frame. Typical observed modes of façade deterioration are presented below.

Differential Expansion

In transitional masonry structures, the masonry wythes, structural frame, and intermediate steel supports (lintels, relieving angles, etc.) are all rigidly bound together despite their differing

characteristics of expansion. Fired clay materials, such as terra-cotta and brick, experience irreversible expansion over time from exposure to water or humid air (BIA, 2006). Steel members experience elastic deformation in the form of horizontal and vertical deflection due to imposed loading conditions or foundation settlement. The differential expansion and movement of the materials imparts stress on the façade, manifesting in masonry cracks and displacement.

A condition commonly observed in transitional facades is the lack of a movement joint underneath the steel shelf angle at each floor level. As such, the shelf angle cannot deflect to carry loads as it was intended to and instead bears directly onto the masonry beneath it. This causes a stacking effect in the exterior walls with gravity loads from units above the shelf angle completely bypassing the angle and instead bearing on the lower wythes of masonry. Stacked curtain wall systems tend to carry some portion of the gravity floor load because walls in axial compression are much stiffer than beams in flexure (Friedman, 1995). Strain-relief testing programs have been performed on the exterior walls of high rise structures, which have determined measured stresses over two hundred times the design value (Stockbridge, 1983). Under this stress, the outer wythe of masonry will eventually crack, spall, or buckle.

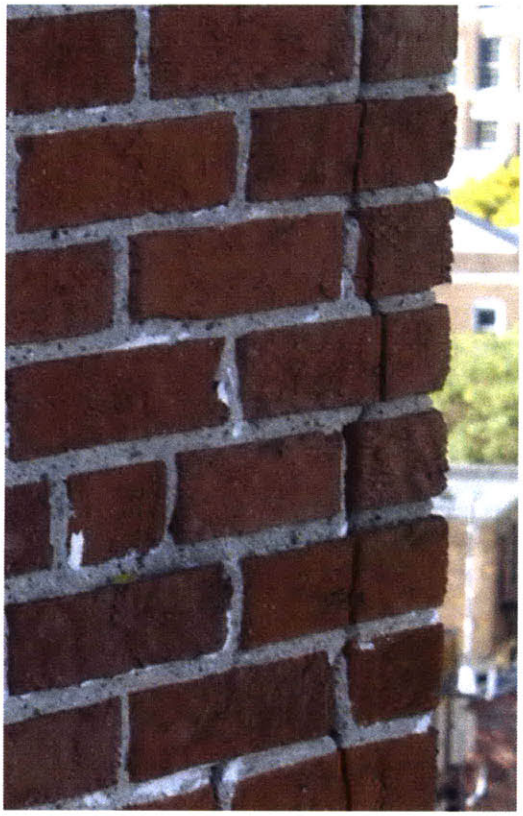

Brickwork on each side of perpendicular walls will expand toward the corner. Without accommodation for this movement, stress will accumulate causing a continuous vertical crack to propagate at the corner, where an expansion joint would typically be recommended in modern curtain wall construction. Lateral wind loading can also induce this cracking. The wall experiencing out-of-plane loading will deflect considerably more than the relatively stiff in-plane masonry wall under uniform lateral pressure, causing large accumulation of stress along the vertical plane at the corner (Friedman and Oppenheimer, 2007). Figure 5 depicts this condition in the façade of the Courtyard Marriot in Boston, MA, a transitional high rise constructed in 1925.

Figure 5: Corner Crack without Expansion Joint

Corrosion of Embedded Steel

Transitional masonry structures rely on the multi-wythe masonry wall for thermal and moisture protection. This results in an environment where the encased structural steel framing is continuously in contact with moisture drawn in by the porous masonry. Façade defects, such as cracks caused by differential movement, serve to further exacerbate the issue as they allow another path for moisture to enter the wall assembly. In addition to reducing the structural capacity of the embedded frame, the volume of steel will greatly increase due to corrosion product in a process called rust-jacking. Rust-jacking puts stress on the tightly fit masonry and can cause cracking and displacement. Figure 6 shows a continuous vertical crack in the outer wythe of masonry on a transitional masonry structure in Boston; a subsequent test cut revealed a corroded steel column.

Figure 6: Cracked Masonry due to Differential Expansion and Rust-jacking of Embedded Steel Column

In transitional masonry façades, continuous vertical crack patterns will be often be observed at column line locations. If masonry cracking is not observed, it does not necessarily mean that the underlying steel frame is in good condition. Due to variations in construction, gaps may have inadvertently been left between the structural system and the masonry infill in some locations, in which case rust-jacking may have less of an effect on the façade.

Secondary steel members such as lintels and shelf angles are typically the first to corrode because they are closest to the exterior masonry wythes that draw in the exterior moisture (Searls and Bronski, 2000). An embedded window lintel that has experienced corrosion deterioration is depicted in Figure 7. Secondary steel members are more susceptible to failure by corrosion because they have thinner webs and flanges, while larger primary columns and girders can typically withstand a much larger loss in section (Dam, 2006).

Figure 7: Deteriorated Secondary Structural Framing

Wall System Connectivity

The aforementioned issues can result in a loss of connectivity between the outer wythe of masonry (terra-cotta, stone, or face brick) and the back-up infill wall. Accumulated stress can cause shear failure of the brick masonry headers tying the outer wythe of masonry to the back-up wall, resulting in reduced out of plane lateral restraint and potential bulging of the exterior wythe (Searls and Bronski, 2000). Exposure to moisture can also cause premature failure of steel anchors supporting decorative terra-cotta pieces, which are typically anchored to the steel super structure via steel rods or square stock, as shown in Figure 8

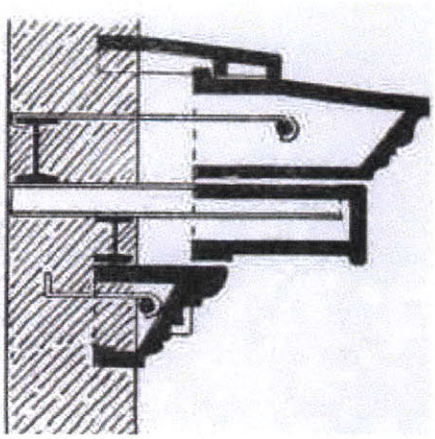

Figure 8: Terra-cotta Cornice
Source: Cyclopedia of Architecture, 2010

(Kidder, 1906). Uncoated steel masonry ties are extremely susceptible to failure from corrosion because of their small section area.

Thermal Performance

Historically, heating and cooling systems were not used in load-bearing masonry structures and heat transfer was regulated by the high thermal mass of the masonry walls and the low window-to-wall ratios. The total insulating resistance (R-value) of a transitional brick masonry wall assembly is usually less than 4 (SI units, $°F \cdot ft^2 \cdot h/BTU$), well below modern standards. Reduction in energy consumption and thermal comfort are two pertinent issues that come up during retrofits. However, adding insulation to a multi-wythe masonry wall has the potential to adversely affect the dynamics of the wall assembly, further encouraging corrosion and deterioration of the embedded steel components. The thermal and moisture performance of a transitional masonry high rise with and without insulation is presented and discussed in Chapter 5.

2.4 Modern Curtain Wall Systems

Many of the flaws inherent in transitional construction were addressed when the modern curtain wall system developed in the 1950s, which is very similar to the form still in use today. Much like transitional masonry structures, the façade is not intended to carry any building loads and is supported by the primary building structure. Unlike transitional facades, modern curtain walls are either face-sealed or incorporate a drainage plane intended to prevent moisture from reaching the underlying structural frame. They are detailed with strategically placed expansion joints to allow for differential movement of the various materials. Wall claddings are considerably thinner and constructed of a wide variety of materials, including aluminum, glass, brick veneer, or thin stone. Modern curtain walls utilize insulation layers and air/vapor barriers within the wall assembly to control air, heat, and moisture transfer. When properly designed and constructed, these structures are more effective at protecting the integrity of the underlying steel frame as well as the cladding. This system has also allowed architects considerable freedom with window-to-wall ratios, which can adversely affect the energy performance of the structure. However, a discussion of the performance and limitations of the modern curtain wall system is not included in this text.

2.5 Façade Ordinance Laws

Even in the early twentieth century, critics of steel frame construction voiced concerns that embedding columns in exterior masonry façades would adversely impact long term building performance. However, after a report was released in 1903 stating that the frame of a transitional masonry structure was in good condition after five years of use, this issue disappeared from the public eye (Friedman, 2009). In reality, the deficiencies in this construction method have taken decades to manifest themselves. Lack of public knowledge meant that the these structures were not carefully monitored or maintained until an accident occurred in New York in 1979 when a college freshman was killed by a piece of masonry that fell from a historic high rise. This event precipitated the creation of Local Law 10, requiring all buildings of more than six stories to receive examination by a licensed engineer at regular intervals (Friedman, 1995). In the years following the adoption of this law, the cities of Boston, Chicago, Columbus, Detroit, Milwaukee, Philadelphia, Pittsburgh, and St. Louis have all signed similar ordinances into effect. The requirements and procedures for conducting façade inspections are outlined in ASTM E2270, "Standard Practice for Periodic Inspection of Building Façades for Unsafe Conditions" (Façade Ordinances, 2010). In addition to helping to protect public safety, façade ordinance laws have enabled engineers and architects to closely examine masonry high rise structures, providing valuable information regarding their mechanisms of deterioration.

2.6 Conclusion

The deterioration mechanisms of transitional masonry façades have been well documented in technical literature, which is partly a result of recently implemented laws for periodic façade evaluations of these structures. The only way for a design professional to gain experience and knowledge about these façades is by reviewing existing literature and historic building plans, preferably in conjunction with hands-on field evaluations. Hygrothermic modeling of wall assemblies, which will be presented for a case study transitional masonry wall in Chapter 5, is a useful way to predict thermal and moisture performance of these structures but this also has limitations. The restoration community would greatly benefit from additional research and detailed analysis of the building materials and envelope systems of transitional masonry buildings, in order to continue to understand underlying sources of deterioration.

3. Structural Analysis Methods

The contribution of exterior masonry cladding to a structure's lateral load capacity was traditionally neglected in the design of early generation high rise buildings. In reality, thick masonry curtain walls are much stiffer in resistance to lateral loads than the semi-rigid steel moment frames they surround and consequently will absorb more of the load. Under moderate wind loading, a simple equilibrium analysis will usually determine that the masonry stress is within allowable limits. Of more concern when evaluating structural health is how the masonry infill and surrounding steel frame will interact under more severe lateral load conditions such as earthquakes.

Compared to a bare frame, the presence of masonry infill reduces the natural period of vibration of the structure and increases the amount of base shear it can withstand. Masonry infills have great potential for strengthening the lateral load resistance of a structure if properly detailed, as has been documented in various analytical studies and experimentation (Dawe and Seah, 1989, Shing et al., 2009, etc.). However, masonry infill can also adversely affect structural stability, as was seen in Turkey after the 1999 earthquakes caused catastrophic failures of many concrete frames infilled with URM. If the characteristically brittle masonry infill fails during a seismic event, the weaker and more flexible surrounding frame will have to absorb the lateral forces and potential impact effects from the infill. Masonry infills can also over-strengthen the upper stories of a structure while inducing a soft lower storey, which is highly undesirable for earthquake resistance (Shing, 2002).

Structure-masonry infill interaction has been a heavily studied field over the past several decades, but there is no consensus on a method to apply to the analysis of these structures. Sophisticated methods of analysis are computationally expensive and might not be practical to implement in a workplace. Many design practitioners choose to neglect the contribution of the masonry infill when structurally analyzing transitional masonry high rise buildings. This results in inaccurate predictions of structural stiffness, strength, ductility, and failure modes, and potentially the implementation of improper retrofit procedures.

This Chapter will begin by presenting the behavior and failure mechanisms of masonry infills under lateral loading. The available methods for analyzing masonry infill will be discussed, based on a literature review of experimental and analytical studies on this topic. The final section of this Chapter will outline how modern building codes address masonry infill walls and discuss options available to structural

engineers analyzing existing transitional masonry structures. This leads into Chapter 4, when these procedures will be illustrated through the structural analysis of a case study transitional masonry wall.

3.1 Failure Modes of Masonry Infilled Frames

Masonry infilled frames exhibit a complex and nonlinear response to lateral loading. Several issues contribute to the difficulty of analyzing infilled frames: the brittle and anisotropic nature of the masonry, the ductile nonlinear characteristics of the frame, uncertainties regarding material and geometric properties, variable conditions at wall-frame interfaces, and interactions between in-plane and out-of-plane loading (El-Dakhakhni, 2002). Except for low levels of lateral loading, the resistance of an infilled frame is not equal to the simple sum of the rigidities of the infill and bounding frame because infill-frame interaction can alter the load-resisting mechanisms of each component (Shing, 2002).

In-Plane Loads

Experimental testing and analytical analysis of masonry infill over the past several decades has resulted in the classification of five different in-plane failure modes, as shown in Figure 9 (El-Dakhakhni et al., 2003):

a. Corner crushing mode (CC mode): Crushing of the infill in at least one loaded corner. This mode exhibits a diagonal strut mechanism, and is typically associated with weak masonry infill surrounded by a frame with weak joints and strong members.
b. Sliding shear mode (SS mode): Horizontal sliding shear failure through bed joints at the mid-height of the infill. This mechanism is associated with an infill with weak mortar joints surrounded by a frame with strong joints and members. Plastic hinges can form at the mid-height of the frame.
c. Diagonal compression mode (DC mode): Crushing of the infill within its central region. This mode is associated with a slender infill with failure resulting from out-of-plane buckling instability.
d. Diagonal cracking mode (DK mode): A crack connecting the two loaded corners. This mode is associated with strong masonry infill surrounded by a frame with weak joints and strong members.
e. Frame failure mode (FF mode): Plastic hinge formation in the columns or beam-column connections, tension failure in the windward column, or compression failure in the leeward column. This is associated with a strong masonry infill surrounded by a weak frame.

Studies have indicated that only the first two modes, the CC and SS modes, are of concern in the analysis of steel-framed transitional masonry high rise buildings and the other three failure modes are not expected to occur (El-Dakhakhni et al, 2003).

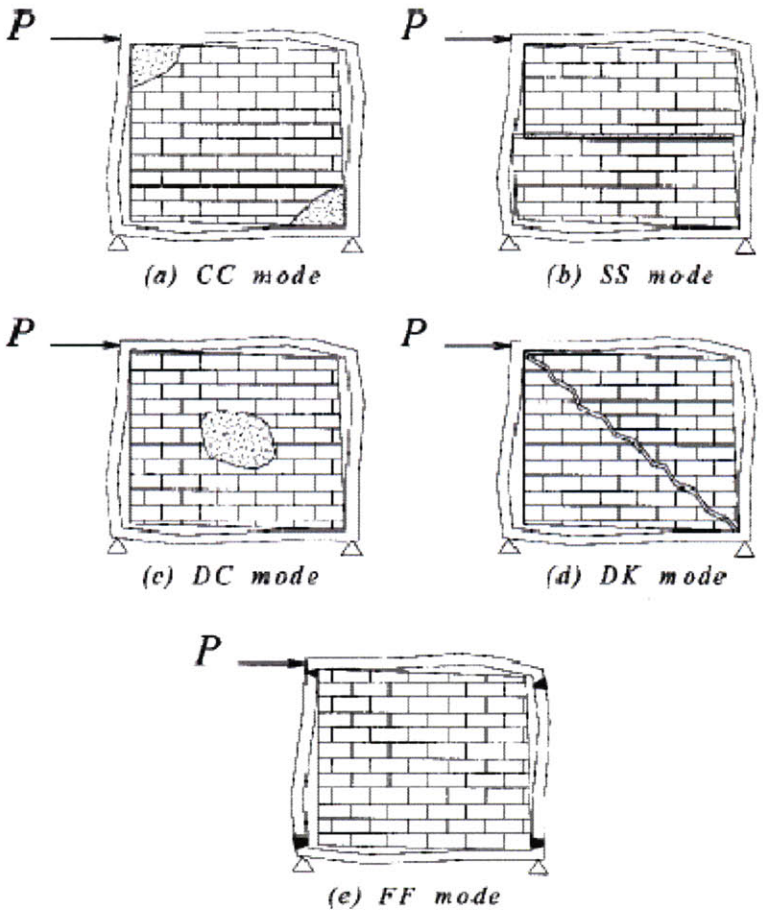

Figure 9: Failure Mechanisms of Infilled Frames
Source: El-Dakhakhni et al., 2003

Out-of-Plane Loads

Out-of-plane failure has been identified as a potential failure mode for masonry infilled frames, particularly in upper stories of high-rise buildings (FEMA, 1998). Analytical and experimental models have been developed to assess the performance of infilled frames under out-of-plane loading, but this is not covered under the scope of this text.

3.2 Analysis Methods

There are a wide variety of methods to analyze the behavior of masonry infill under lateral loading. Approximating the masonry infilled frame as a cantilevered beam using classical masonry analysis can

provide a reasonably accurate estimate of stiffness within the elastic material range. More sophisticated methods of analysis can either be classified into two theorems of limit state – Lower Bound and Upper Bound. The actual unique failure condition will fall somewhere between these two bounds. The Lower Bound theorem, also called the "safe theorem", postulates a set of forces in equilibrium that do not violate plasticity. This can be equated to allowable stress design in modern structural analysis, a solution which is in equilibrium and satisfies the yield condition but does not correspond to a mechanism of collapse. However, members can usually carry loads after the commencement of yielding. The Upper Bound theorem, also called the "unsafe theorem", states that if a loading is found that causes a collapse mechanism to form then that loading must be greater than or equal to the collapse load. The methods listed below, with exception of the cantilever beam model, provide upper bound estimates of the collapse load of the infilled frame because they take into account plastic behavior after initial yielding.

3.2.1 Stiffness Approximation Method

Cantilever Beam

An approximate method for estimating the stiffness of a masonry infilled frame is to model the wall as a cantilevered beam using classical masonry analysis. Fiorato et al. (1970) proposed using a shear beam model for infill stiffness analysis, and found good correlation with experimental results at low load levels (approximately 10-30% of the ultimate load) (Shing, 2002). This can be a useful simple method to estimate wall performance under low lateral loads. The validity using a cantilever beam model is further explored in Chapter 4.

3.2.2 Upper Bound Analysis Methods

Limit State Analysis

Limit State Analysis design principles have been used by researchers to predict ultimate load of masonry infilled frames, including Liauw and Kwan (1985), Mehrabi et al. (1994), and Saneinejad and Hobbs (1995) (Shing, 2002). The general theory of plastic analysis is that the work done by the forces applied to the structure must be equal to the energy dissipated at plastic hinge locations. According to plastic theory, deformations are lumped at plastic hinge locations on a member while the rest of the system shows linear elastic behavior (Baker and Heyman, 1980). If modes of failure and locations of plastic hinges are accurately predicted, then these relationships can be used to determine a value for a structure's base shear at collapse. This method is further explored in Chapter 4.

Equivalent Strut Macro Model

The simplest and most developed method for the analysis of infilled frames equates the masonry infill to an equivalent pin-jointed diagonal strut. At relatively low load levels, the infill panel will separate from the bounding frame at the windward lower and leeward upper corners, causing compressive contact stress to develop in the region shown in Figure 10. From this point onwards, the in-plane behavior of an infilled frame is distinctly different from a shear wall. Holmes (1961) proposed an effective width for a pin-jointed compression strut that was a function of the thickness and aspect ratio of the infill. Other researchers have since proposed various alternate equations for the equivalent strut width (Shing, 2002). National guidelines for the evaluation existing buildings in North America have adopted the equivalent diagonal strut as the recommended method for analysis of masonry infilled frames, which will be discussed in Section 3.3.

Although computationally attractive, the diagonal strut model has some weaknesses. It only accounts for the CC failure mode but the infill frame could experience other modes of failure. It also does not represent local effects resulting from the interaction between the infill and the frame, making it difficult to predict plastic hinge locations. More complex models have been proposed by subsequent researchers, shown in Figure 11, which incorporate multiple diagonal struts with the intent of representing the actions in the frame more accurately (Teeuwen, 2009).

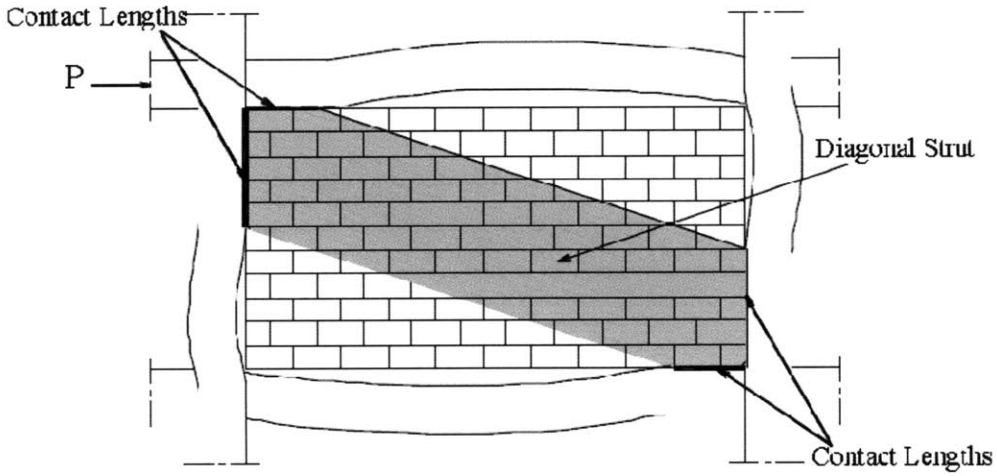

Figure 10: Diagonal Compression Strut Analogy
Source: El-Dakhakhni, 2002

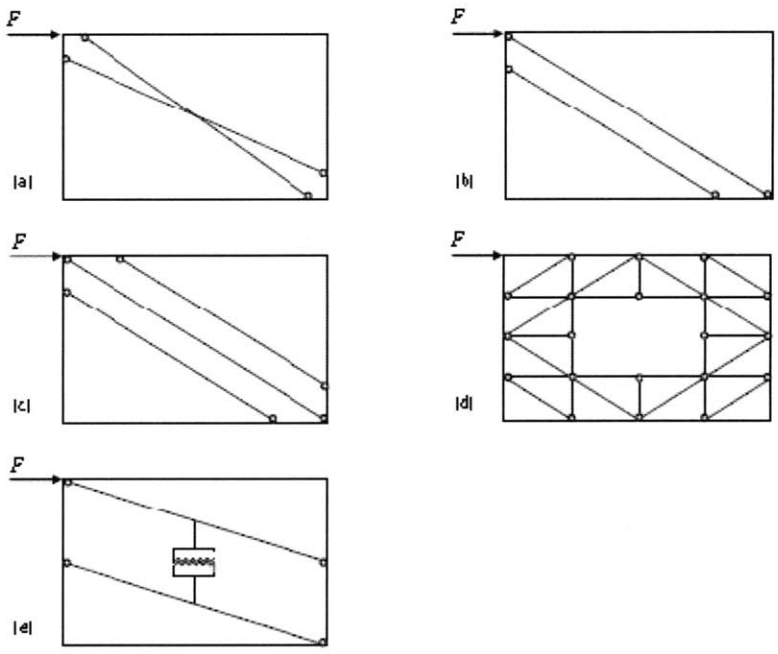

Figure 11: Modified Diagonal Strut Models
Source: Crisafulli et al. (2000) reprinted in Teeuwen, 2009

Finite Element Method

The finite element method (FEM) has become the most common approach for the analysis of masonry infill frame interaction in experimental research along with full-scale testing. There are various different ways in which the masonry panels can be modeled, but can be classified into two distinctive types: infill panels modeled as a homogeneous shell before fracture with the effects of mortar joints smeared out ('smeared crack models') or heterogeneous modeling of masonry using separate elements for the frame, masonry, and interface elements to account for planes of weakness induced by mortar joints (Shing, 2002). Using FEM to analyze structure-masonry wall interaction has the potential to be a very powerful tool if properly implemented as it can potentially analyze all potential failure modes concurrently and consider inelastic responses. However, constructing a finite element model is computationally and time intensive, and improper use can lead to unconservative results.

3.3 Building Code Requirements

If a substantial renovation of an existing building is undertaken, the International Building Code requires that the structure comply with modern building code requirements (ICC, 2006). The American Society of Civil Engineers recently published a new design code, ASCE/SEI-41 *Seismic Rehabilitation of Existing Buildings* (ASCE-41), which provides guidelines on how to assess and strengthen existing buildings. This

standard was developed from the governmental publication FEMA 356 and is a performance-based design code, meaning analysis methods are based on allowable deformations rather than allowable stresses (ASCE, 2006). Displacements are a better indicator of damage in the nonlinear range of building response than forces because in this range relatively small changes in force correspond to significant changes in displacement.

A component by component evaluation of the structure is performed for the selected rehabilitation objective, with each component treated as either a force or displacement controlled element. Four different analysis procedures may be used to establish seismic demands, ranging from least to most accurate:

1. Linear Static Procedure (LSP): The building is modeled with linearly elastic stiffness and equivalent viscous damping values. A "pseudo-lateral load" is calculated from an empirical formula and applied to the structure in a specified distribution. If the building remains elastic during the earthquake, then the calculated forces will be similar to those expected during the event. If the building responds inelastically, which is more likely for a masonry infilled frame, the actual internal forces that develop will be less than those calculated using the pseudo-lateral load (ASCE, 2006). This procedure is intended to be simple and very conservative, and is not applicable for all building types.

2. Linear Dynamic Procedure (LDP): This procedure also assumes linearly elastic stiffness and equivalent viscous damping values. A modal spectral analysis is carried out using a site-specific linear elastic response spectrum is then used to find internal displacements and forces. Much like the LSP, calculated forces will typically exceed those that the building can sustain due to expected inelastic response of components (ASCE, 2006).

3. Nonlinear Static Procedure (NSP): Commonly referred to as a 'push-over analysis', a numerical model is created that directly incorporates nonlinear load deformation characteristics of building components, which is subjected to increasing lateral loads until a target displacement is exceeded. Accounting for nonlinear behavior results in internal forces that are much closer approximations of those expected in a design earthquake. Lateral loads are applied in proportion to the distribution of inertia forces proportional to the shape of the fundamental mode. Generalized force-deformation relationships for building components are provided in the

standard. As shown in Figure 12, five points labeled A, B,C, D, and E are used to define the force deformation behavior of a plastic hinge and the three points labeled IO, LS, and CP are used to define the acceptance criteria. IO, LS, and CP stand for Immediate Occupancy, Life Safety, and Collapse Prevention respectively. The NSP will be further discussed in Chapter 4, including how to generate force-displacement relationships for components of a masonry infilled structure.

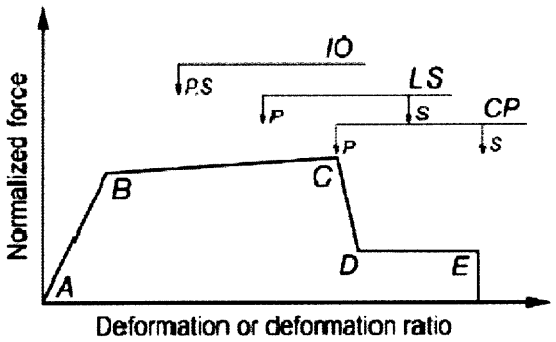

Figure 12: Generalized Force-Deformation Relationship
Source: ASCE, 2006

4. Nonlinear Dynamic Procedure (NSP): The NSP involves creating a finite element model of the building that directly incorporates nonlinear load deformation characteristics of building components, and subjecting it to earthquake shaking from a time-history analysis to determine forces and displacements (ASCE, 2006). This is the most accurate method for determining building response, however it is computationally expensive to model the anisotropic properties of masonry in a discretized finite element model.

Masonry Infill

ASCE-41 states that masonry infill panels shall be considered primary elements of the structure's lateral force resisting system and as such are integral to the seismic assessment. For both steel and concrete infilled frames, the standard recommends analyzing the composite system until the point that the wall is determined to fail. At this point, the wall shall be removed from the analytical model and analysis shall continue on the bare frame. To calculate in-plane stiffness and strength, the standard recommends creating a nonlinear finite element model of the composite system. However, it does not provide any guidance on how to model the masonry in finite element software, which is well known as being an extremely complicated and sensitive task. Alternatively, the standard says that the masonry can be

modeled as an equivalent diagonal compression strut of width a, given by the following equation (ASCE, 2006):

$$a = 0.175(\lambda_1 h_{col})^{-0.4} r_{inf} \qquad \textbf{(Eq. 3-1)}$$

Where

$$\lambda_1 = \left[\frac{E_{me} t_{inf} \sin 2\theta}{4 E_{fe} I_{col} h_{inf}}\right]^{\frac{1}{4}}$$

And

h_{col} = column height between centerlines of beams (in.);

h_{inf} = height of infill panel (in.);

E_{fe} = expected modulus of elasticity of frame material (ksi);

E_{me} = expected modulus of elasticity of infill material (ksi);

I_{col} = moment of inertia of column (in^4);

r_{inf} = diagonal length of infill panel (in.);

t_{inf} = thickness of infill and equivalent strut (in.);

θ = angle whose tangent is the infill height-to-length aspect ratio (rad)

The full procedure of how to analyze a masonry infilled structure is not described under the scope of this text, but the case study in Chapter 4 will highlight key elements of this method. The standard requires the engineer to check local effects resulting from the infill strut force on the frame adjacent to the infill panel to ensure this is not a failure mode, addressing one of the shortcomings of the strut-model method previously discussed.

If materials testing cannot be performed on the existing structure being analyzed, ASCE-41 provides tables listing default lower-bound material strengths. The values for steel are appropriate as they have been taken from historic catalogues from steel manufacturers, meaning there is little room for error. The masonry lower bound properties are conservative. Table 1 lists compressive strength in pounds per square inch (psi) for various kinds of brick, published in a 1914 text based on tests performed in Watertown, Massachusetts. Table 2 lists the compressive strengths recommended by ASCE-41, which are lower by almost an order of magnitude. It is important to incorporate very high factors of safety when working with historic masonry due to its brittle and anisotropic nature. However, being too conservative might result in underestimation of building strength and unnecessary retrofit intervention.

If at all possible, it is recommended to perform prism testing to determine brick compressive strength in accordance with ASTM C1314, which accepted by the code as an alternate procedure. If testing is not an option, the engineer must use sound judgment when estimating the strength of the masonry in question.

TABLE 8.

COMPRESSIVE STRENGTH OF BRICK MANUFACTURED BY DIFFERENT PROCESSES AT DIFFERENT PLACES.

Rep. No.	Kind of Brick.	Compressive Strength, Pounds per Square Inch.		
		Min.	Max.	Mean.
	FACE BRICK:			
1	Stiff-mud	8 930	15 330	12 766
2	Dry-pressed	8 930	17 990	11 190
3	Re-pressed soft-mud	5 770	7 560	6 780
	COMMON BRICK:			
4	Hard-burned, soft-mud, Cambridge	9 140	14 750	11 340
5	" " " " Brookfield	4 340	4 580	4 475
6	" " " " Mechanicsville	5 110	6 730	5 808
7	Medium-burned, soft-mud, Cambridge	4 610	8 590	6 590
8	" " " " Brookfield	4 200	6 850	5 248

* Tests of Metals, etc., 1894, p. 456–68.
† *Ibid.*, 1904, p. 453–54.

Table 1: Compressive Strength of Brick
Source: Baker, 1914

Table 7-1 Default Lower-Bound Masonry Properties

	Masonry Condition[1]		
Property	**Good**	**Fair**	**Poor**
Compressive Strength (f'_m)	900 psi	600 psi	300 psi
Elastic Modulus in Compression	$550f'_m$	$550f'_m$	$550f'_m$
Flexural Tensile Strength[2]	20 psi	10 psi	0

Table 2: Lower-Bound Masonry Properties
Source: ASCE, 2006

3.4 Conclusion

Evaluating the strength and performance of masonry infilled frames is a difficult task. If done improperly, it can result in incorrect predictions of strength and performance. Incorporating the nonlinear properties of the frame and infill will provide a much more accurate prediction of failure mode and strength. These concepts will be further developed in the next section through a case study.

4. Structural Analysis of Transitional High Rise Case Study

This Chapter presents the results of a structural assessment of a fictional transitional masonry high rise building located in Boston, Massachusetts. First, a nonlinear static pushover analysis was performed on a two-dimensional model of a typical bay of the building (shown in Figure 15) to evaluate the contribution of the masonry infill and determine the earthquake response of the system. Diagonal struts were used to model the stiffness contribution of the masonry infill in accordance with the Equivalent Strut Macro Model introduced in Chapter 3. Next, cantilever beam modeling and limit state analysis methods were performed on the same structure to assess the validity of these more approximate and less computationally expensive methods. Multiple full elevation models with different infill configurations were then evaluated using a nonlinear pushover analysis, in order to determine the effects of various infill configurations on the performance of the structure. Finally, the results of the different analysis methods are presented and discussed.

4.1 Prototype Building

The focal point of the study is a prototype building typical of early twentieth century high rise construction. The structure has a steel frame with semi-rigid moment connections and unreinforced brick masonry infill walls. The floor system is a rigid reinforced concrete slab. A detail of the wall assembly is shown in Figure 13. A plan view of the structure and the elevation view of one bay of the masonry infilled frame are shown in Figure 14 and Figure 15 respectively.

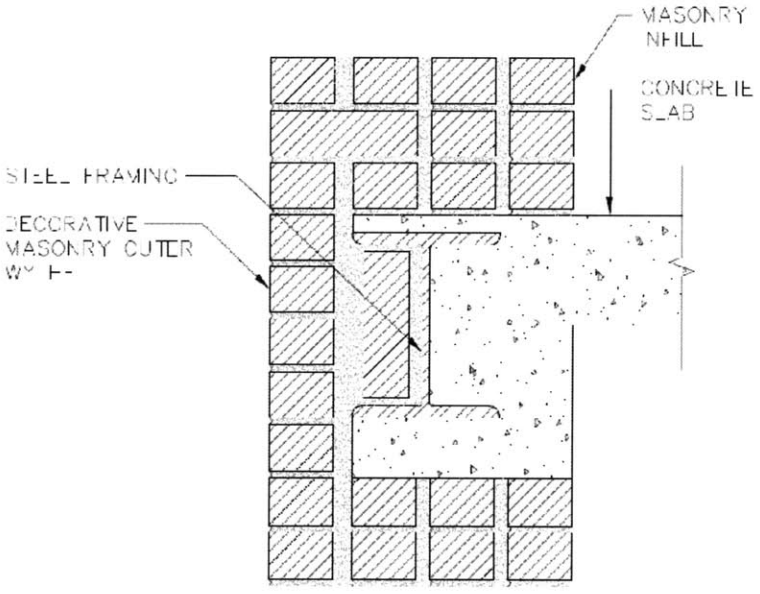

Figure 13: Detail of Prototype Wall Assembly

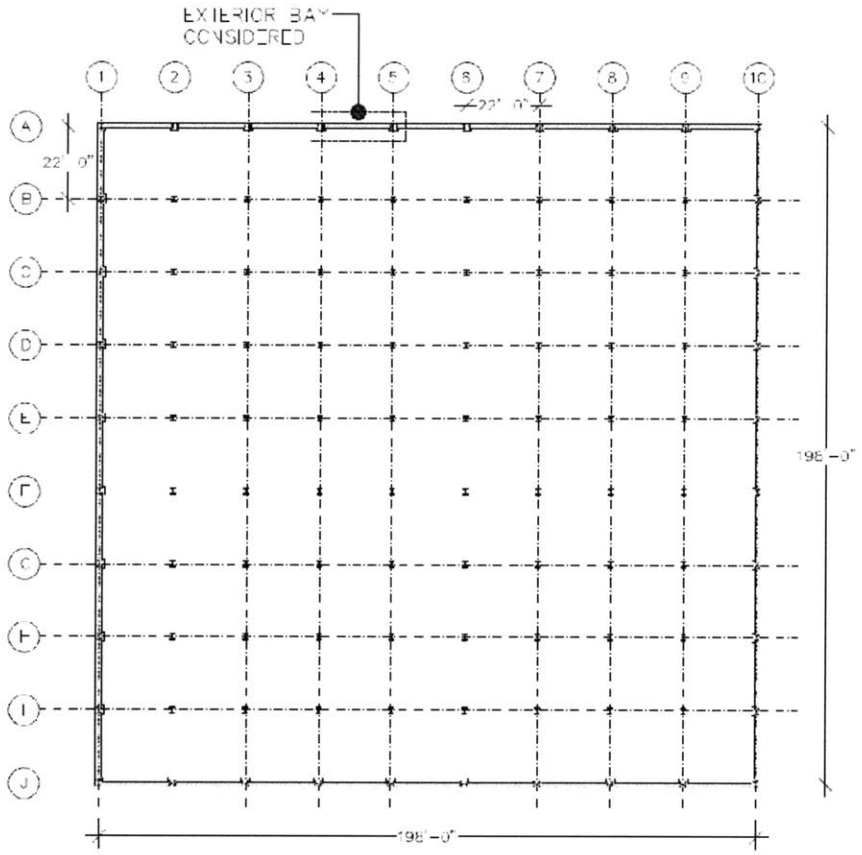

Figure 14: Plan View of Prototype Building

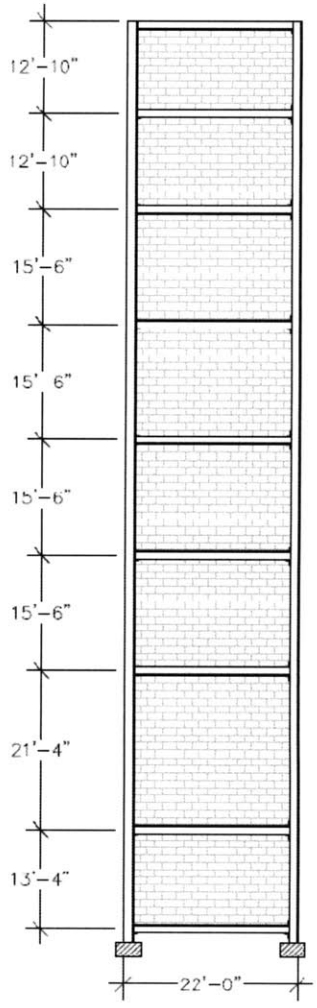

Figure 15: Elevation view of Typical Bay

In accordance with engineering practice of the time period, the steel structure was designed for gravity loads only, which includes self weight, concrete floor slab, masonry infill, parapet wall, interior finishes, and live load. Assuming a public assembly use group, the design live load was taken as 100 pounds per square foot (psf) for the interior floors and 40 psf for the roof. The structure was designed using modern allowable stress design procedure (AISC-ASD01) with historic member properties and present-day section properties.

4.1.1 Nonlinear Numerical Model

For the pushover analysis, it was necessary to construct a model that would incorporate nonlinear load deformation characteristics of the building components. The structural analysis software SAP2000 Advanced v11.0.0 (SAP2000) was used to create two-dimensional frame models of the prototype building. Nonlinear behavior is represented in SAP2000 by user-defined hinges which form when the

entire cross section of a member has reached yield capacity in accordance with the plastic hinge hypothesis discussed in Section 3.2. Hinges can be assigned to a frame element at any location along the element. This will be discussed in further detail later in this section.

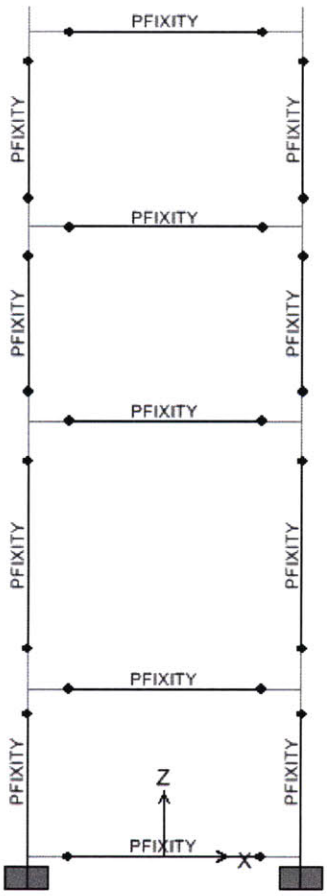

Frame elements were used to represent beams and columns, and the masonry infill was modeled as a pair of diagonal elements for each panel. A rigid diaphragm was input at each floor level to represent the concrete floor slab, allowing for free vertical displacements at each node and collective horizontal motion of all in-plane nodes. Joint masses corresponding to the dead load were input at each node for the modal analysis. Joint releases were modeled as partially fixed to represent the semi-rigid moment connections in the prototype structure. In SAP2000, the user has the option of specifying a partial fixity factor when choosing joint releases, which is a relationship between the moment and the rotation at the connection. Partial fixity values of 500,000 kip-ft/radian were specified at each joint, as shown in Figure 16. Although in modern design, the moment-resisting capacity of these connections would be ignored, research has shown that these connections are capable of contributing non-negligible stiffness through very large drift demands, so it was necessary to represent this accurately in the numerical model (ASCE, 2006).

Figure 16: SAP2000 Model of Semi-rigid Frame

Frame Hinges

Plastic hinges were generated in SAP2000 for the beam and column elements assuming a deformation controlled (ductile) failure. The nonlinear frame elements consists of PMM-hinges (P-axial force, MM-biaxial moments) for columns and M3-hinges (uniaxial moment) for beams. The modeling parameters of the hinges were calculated from values specified in ASCE-41 for partially restrained moment connections, assuming Limit State 1. In

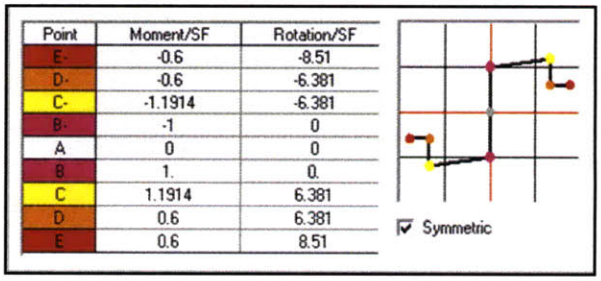

Figure 17: SAP2000 User Defined M3-hinge

reality, ASCE-41 requires that the engineer check four different limit states for each connection, and the lowest calculated moment strength would be used when constructing the force-deformation curve. SAP2000 imports default hinge properties, which can then be manually edited by the user. Figure 17 shows an M3-hinge configured specifically for the prototype structure. Note that the moment and rotation values are divided by a scale factor (SF), which SAP2000 automatically assigns to be the yield moment and rotation value unless otherwise specified by the user. Hinges were assigned at both ends and the center span of each member where the largest moments are expected.

Strut Hinges

The masonry infill is represented with an equivalent diagonal compression strut whose geometric properties were calculated based on Equation 3-1, provided in ASCE-41. Calculations can be found in Appendix B. The compression strut is modeled in SAP2000 with a deformation-controlled P-hinge (axial) with zero tensile strength. The infill strength properties along the diagonal plane will be different than the vertical and shear strengths, as illustrated in the orthotropic model of a masonry panel shown in Figure 18. The strength properties of the panel in the diagonal direction were determined based on a procedure outlined by El-Dakhakhni et al. in 'Three-Strut Model for Concrete Masonry Infilled Frames' (2003). Because the panel behaves as if it were diagonally loaded, constitutive relations of orthotropic plates and axes of transformation matrix are used to obtain the Young's modulus, E_θ, of the panel in the diagonal direction using the following equation (El-Dakhakhni et al., 2003):

$$E_\theta = \frac{1}{\frac{1}{E_0}cos^4\theta + \left[-\frac{2v_{0_{90}}}{E_0} + \frac{1}{G}\right]cos^2\theta sin^2\theta + \frac{1}{E_{90}}sin^4\theta} \qquad \textbf{(Eq. 4-1)}$$

The estimated Young's modulus is related to the ultimate compressive strength (f'_{m_θ}) using the same factor that relates Young's modulus perpendicular to the head joint (E_{90}) to the vertical ultimate compressive strength (f'_{m_90}), neglecting the shear stress effect because the infill is failing in the CC mode. The procedure assumes that the secant Young's modulus at peak load E_p is equal to half the initial Young's modulus E_θ. As shown in Figure 19, now that E_p and f'_{m_θ} are known, it is a simple task to determine the strain corresponding to the peak load ε_p. The stress-strain curve is approximated with a tri-linear relationship, assuming the following parameters:

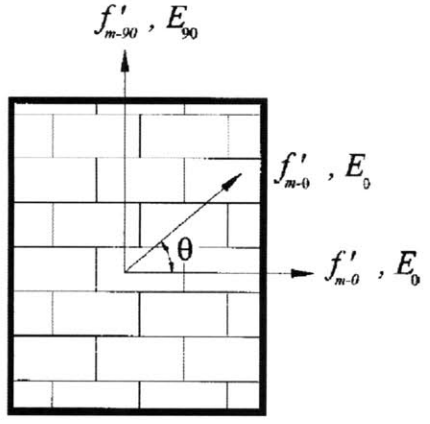

Figure 18: Orthotropic Model of Masonry Panel

$$\varepsilon_1 = \varepsilon_p - 0.001 \qquad \text{(Eq. 4-2)}$$

$$\varepsilon_2 = \varepsilon_p + 0.001$$

$$\varepsilon_u = 0.01$$

Knowing the area and length of each diagonal strut makes it possible to transform this into a force-deformation relation, as shown in Figure 19. A user specified P-hinge can then be customized in SAP2000 for the calculated force-deformation curve, as shown in Figure 20. In this case, the scale factor (SF) was defined to be unity. To prevent numerical instabilities, the hinge was modified in such a way that the compressive strength is equally divided in tensile and compressive zones. Then, a nonlinear tension limit of zero was assigned to each strut in SAP2000 to represent the negligible tensile strength.

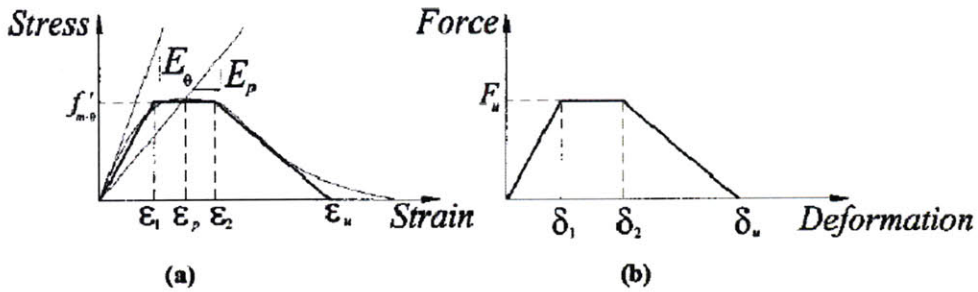

Figure 19: (a) Stress Strain (b) Force-Deformation Simplified Trilinear Relations

Point	Force/SF	Disp/SF
E-	0	-3.08
D-	-213	-1.19
C-	-213	-0.57
B-	-213	0
A	0	0
B	213.	0.
C	213.	0.57
D	213.	1.19
E	0.	3.08

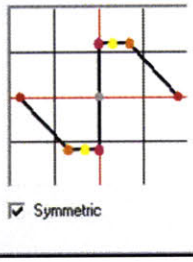

Figure 20: SAP2000 User Defined P-hinge

4.1.2 Pushover Load Case

ASCE-41 requires the lateral load be applied to the numerical model in proportion to the inertial forces in the plane of each floor diaphragm, with the vertical distribution proportional to the shape of the fundamental mode in the direction under consideration (ASCE, 2006). This modal nonlinear load case is specified in SAP2000 to start at the final condition of the dead load nonlinear analysis.

4.1.3 Evaluation Criteria

For the symmetrical geometry of this structure with negligible torsional effects, the damage potential to the entire building can be inferred from the damage pattern of the two-dimensional frame elements. In the ASCE-41 nonlinear static procedure, a target displacement of the control node, located at the center of mass of the roof, is calculated based on site-specific response spectrum. The target displacement is intended to represent the maximum displacement of the structure likely to be experienced during the design earthquake, and is represented by the equation:

$$\delta_t = C_0 C_1 C_2 S_a \frac{T_e^{\,2}}{4\pi^2} g \qquad \textbf{(Eq. 4-3)}$$

Where C_0, C_1, and C_2 are modification factors, S_a is the response spectrum acceleration at the effective fundamental period and damping ratio, T_e is the effective fundamental period of the building in the direction under consideration, and g is the acceleration due to gravity. After the target displacement is calculated, member strengths and story drifts are verified at this value of δ_t. Story drift limits are calculated based on values specified in ASCE/SEI 7-05, *Minimum Design Loads for Buildings and Other Structures* (ASCE 7-05). In order to provide another metric for comparison, the anticipated base shear for the building was also calculated based on ASCE 7-05 procedures. All calculations can be found in Appendix A.

4.2 Pushover Analysis of a Typical Bay

A pushover analysis was performed on a bare frame model (Model 1) and a model with diagonal struts to represent the masonry infill (Model 2), shown in Figure 21. As illustrated in Table 3, the bare frame model significantly overestimates the fundamental period of the structure, while the diagonal strut model is much closer to the approximate fundamental period estimated using ASCE 7-05 methods. This discrepancy highlights the importance of including the effects of the infill when predicting the structure's response. The natural frequency of the structure directly correlates to how it will react to ground accelerations.

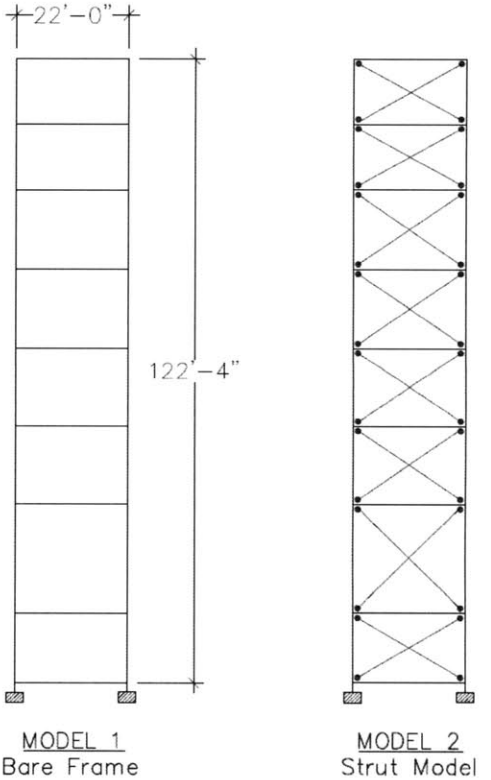

Figure 21: Strut Models

	Model	Fundamental Period (sec)	Expected Displacement under Design Earthquake at Roof (in.)
Bare Frame	1	4.05	17.06
Frame with Diagonal Struts	2	0.91	4.01
ASCE 7-05 Estimate		0.9	

Table 3: Fundamental Period of Models

The base shear versus displacement curve for each model is shown in Figure 22. As expected, Model 2 can withstand much larger base shears while maintaining more stable displacement values because of the contribution of the masonry infill. The target displacement of Model 1 is above allowable drift limits while Model 2 is safely within acceptable range. Model 1 does not have sufficient capacity to withstand the expected base shear, indicated by the green line. Meanwhile, Model 2 is still within linear elastic range at the expected base shear, showing the increased capacity of the infilled model. Linear elastic and collapse limit forces for each structure are shown in Table 4; failure is indicated by the red cells.

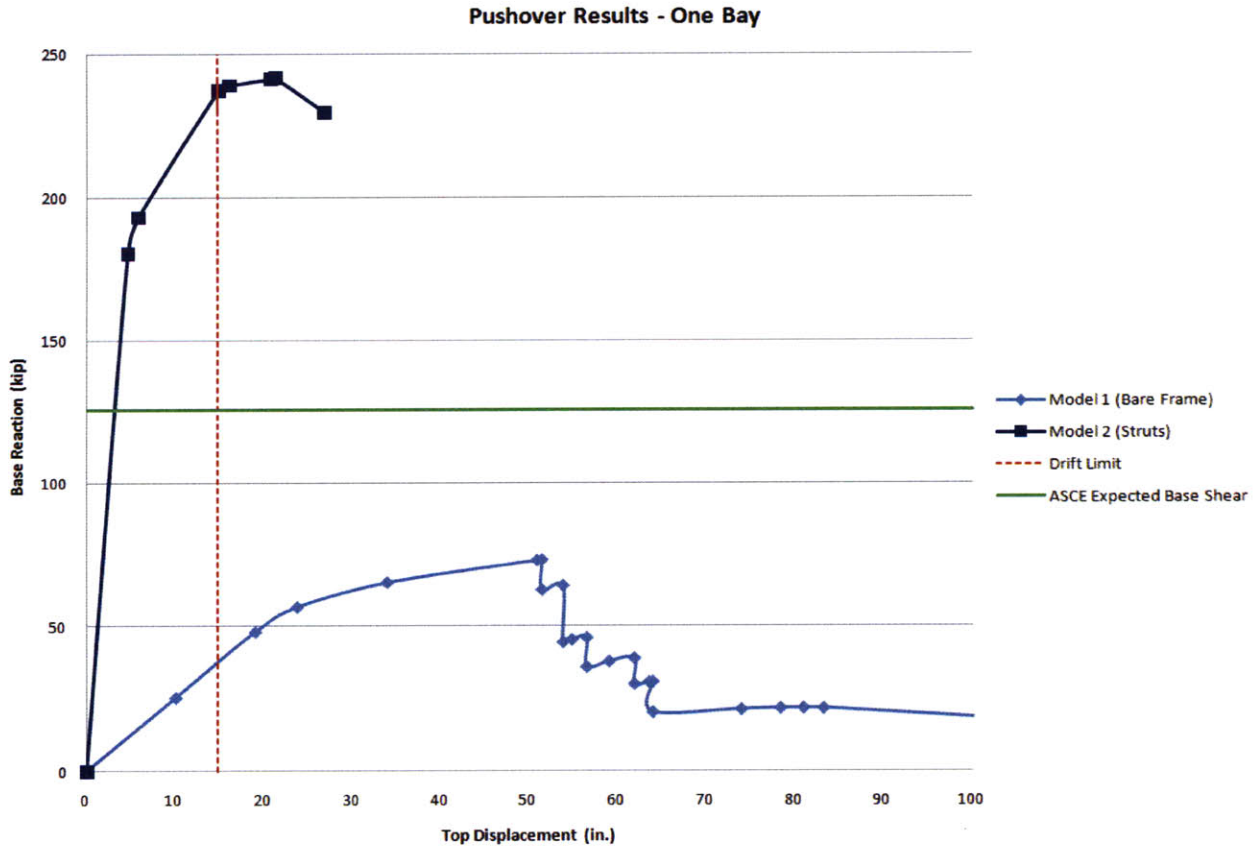

Figure 22: Pushover Curve for Typical Bay

	Model	Base Shear Force (kips)	
		Linear Behavior Limits	Collapse Limits
Bare Frame	1	25	72
Diagonal Struts	2	182	240
Expected Base Shear (ASCE)		**126**	

Table 4: Typical Bay Pushover Analysis Results

Model 1 (Bare Frame) Hinge Formation

Model 1 cannot withstand the expected base shear without the contribution of the masonry infill, as shown in Figure 22 and Table 4. Figure 23(a) shows the structure at its final state before collapse. Failure hinges have formed on the second, third, and fourth stories, represented by the red hinge symbols. Hinge colors represent the hinge's location along the force-displacement curve (shown in Figure 12), and are related to the acceptance criteria; red hinges represent collapse. The corresponding shear force distribution at the point is shown in Figure 23(b). The comparison of the two models shows that the bare frame alone cannot be relied upon as the main lateral force resisting system of the building. Only accounting for its contribution to the resistance will result in an inaccurate prediction of failure.

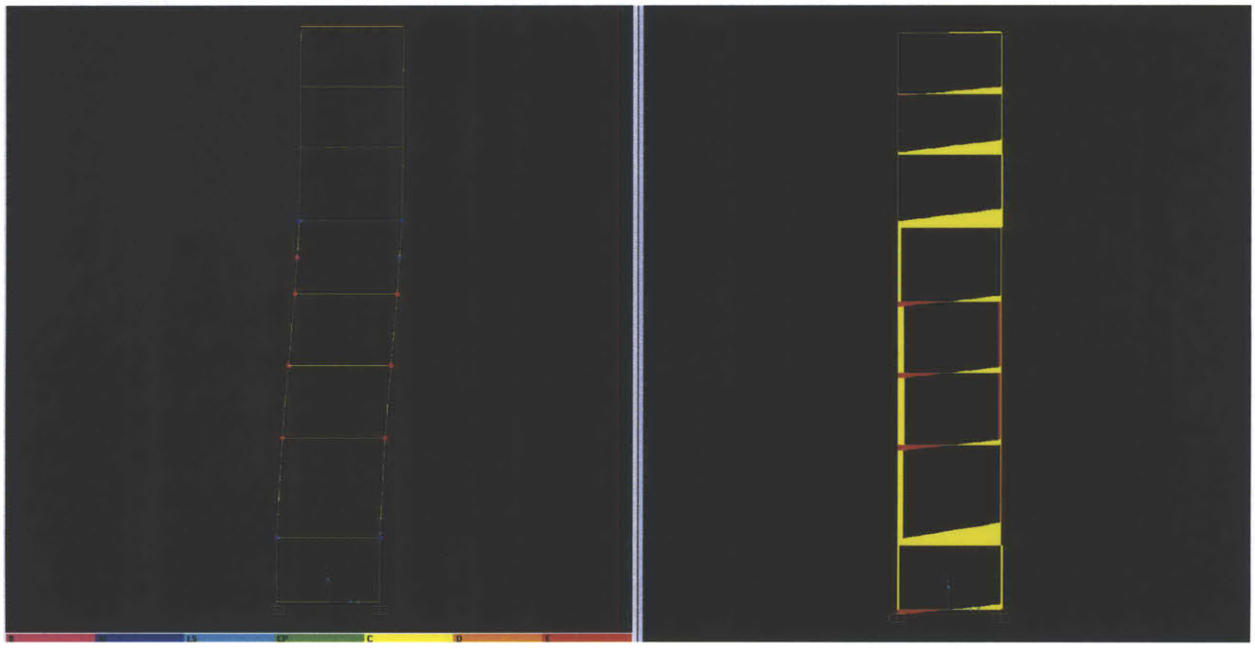

(a) (b)

Figure 23: Bare Frame Hinge formation at (a) Expected Displacement; (b) Failure State

Model 2 (Diagonal Strut) Hinge Formation

The expected displacement of Model 2 under the design earthquake is approximately 4 inches, which occurs at Step 1 of the SAP2000 nonlinear pushover analysis. This also corresponds to the expected base shear value. As shown in the deflected shape diagram in Figure 24(a), only the masonry infill on the second story has yielded and no frame hinges have formed. This indicates that the steel frame will survive the design earthquake intact and only the infill panel will sustain damage. It was observed that the masonry panel on the second story yielded before the first story, which is a result of its larger floor-to-floor height. Figure 24(b) shows the structure in its final state before collapse. Masonry panels on the second through fourth story yield prior to any frame hinge formation, which indicates that up to relatively high load levels, the masonry is acting as the primary lateral load resisting system of the building. Hinges form in the steel frame members on the lower stories before failure of masonry infill or framing on the upper stories, presumably due to higher values of shear force at lower levels. The infilled model performed much better than the bare frame alone, showing the importance of including the masonry infill contribution to calculations of lateral load resistance.

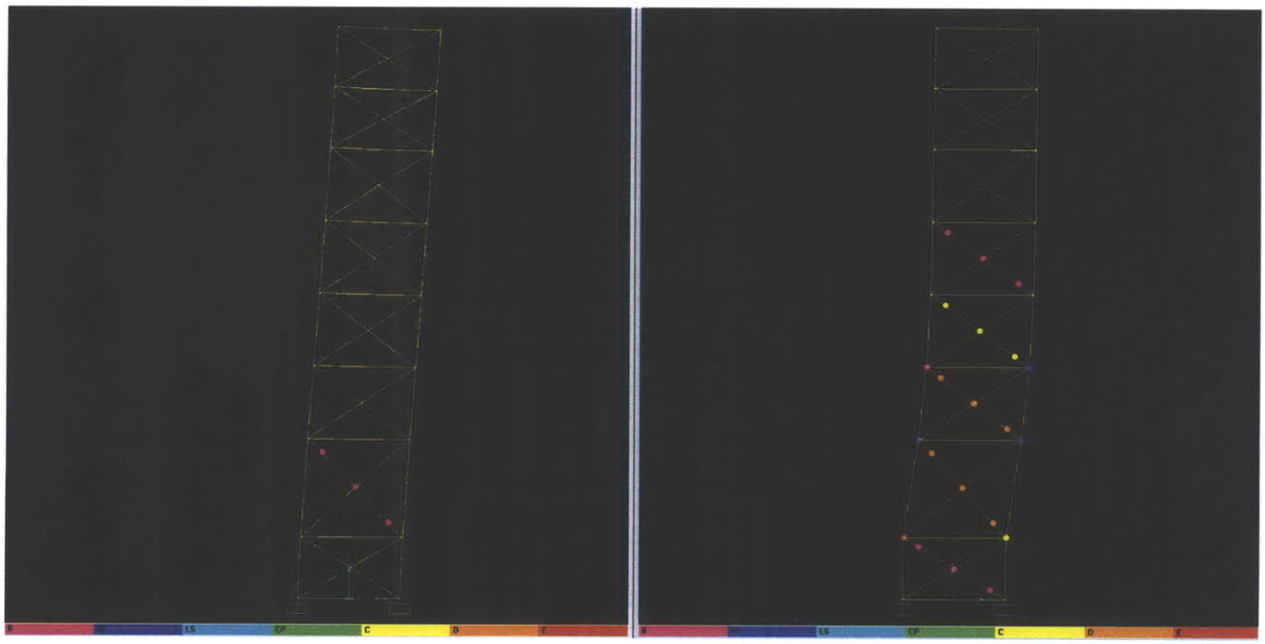

(a) (b)

Figure 24: Infilled Frame Hinge formation at (a) Expected Displacement; (b) Failure State

4.3 Cantilever Beam Model of a Typical Bay

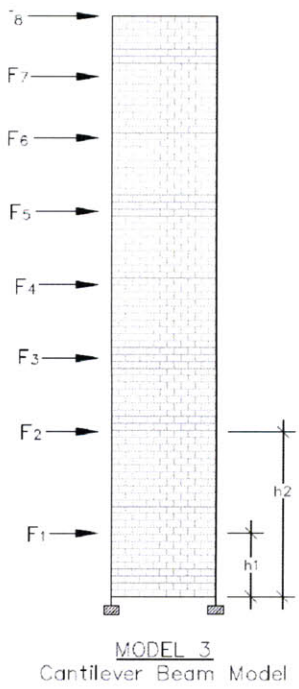

Figure 25: Cantilever Beam Model

The bay was modeled as a cantilevered beam with lateral loads applied at each floor, pictured in Figure 25. Using the Method of Virtual Work, the displacement of the control node was calculated as:

$$\Delta_{roof} = \sum_{i=1}^{n} \frac{h_i^3 F_i}{3EI} + \sum_{i=1}^{n} \frac{F_i h_i}{E_V A} \qquad \textbf{(Eq. 4-4)}$$

In order to compare the cantilever beam model to the pushover analysis from the previous section, displacements were monitored for incrementally increasing lateral loads. For consistency with the pushover model, the vertical distribution of the lateral loads was distributed proportional to the shape of the fundamental mode:

$$F_i = \frac{m_i \phi_i}{\sum_{j=1}^{n} m_j \phi_j} F_b \qquad \textbf{(Eq. 4-5)}$$

Where m_i is the *i*th story mass, F_b is the base shear, and ϕ is the mode shape coefficient for the *i*th floor. Calculations can be found in Appendix C.

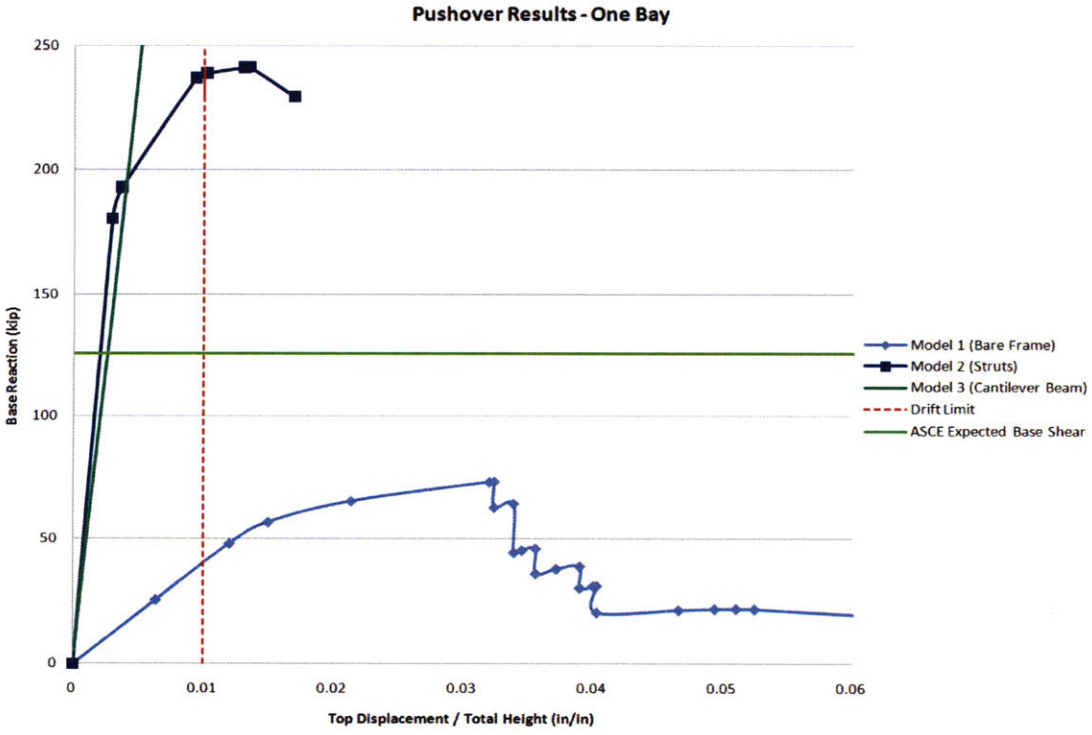

Figure 26: Pushover Curve for Typical Bay with Cantilever Beam Model

As shown in Figure 26, Model 3 (cantilever beam) shows good correlations with the early stages of the pushover curve obtained from Model 2 (strut model). Within the linear range, the slope of the Model 3 force-displacement curve is only a small amount lower than that of Model 2. The slightly larger force-displacement slope of Model 2 can be attributed to the additional stiffness contribution of the steel frame. For a bay of this width and height, the cantilever beam model is appropriate for estimating force-displacement relationships of a masonry infilled wall within the linear range. This method is attractive as it is very simple and does not require the construction of a finite element computer model. However, without constructing the computer model, the yield point of the infilled frame - the point at which linear behavior can no longer be assumed - is not known. Therefore, the cantilever beam model must be used with caution, particularly with brittle infill materials that have low compressive strength. It is most appropriate for low level loads that are not likely to cause material yielding.

4.4 Limit State Analysis of a Typical Bay

The general theory of plastic analysis is that the work done by the forces applied to the structure must be equal to the energy dissipated at plastic hinge locations. First, the ultimate load for a single story frame will be derived using plastic theory. The expected collapse mechanism under a single horizontal load is shown in Figure 27 (Baker and Heyman, 1980).

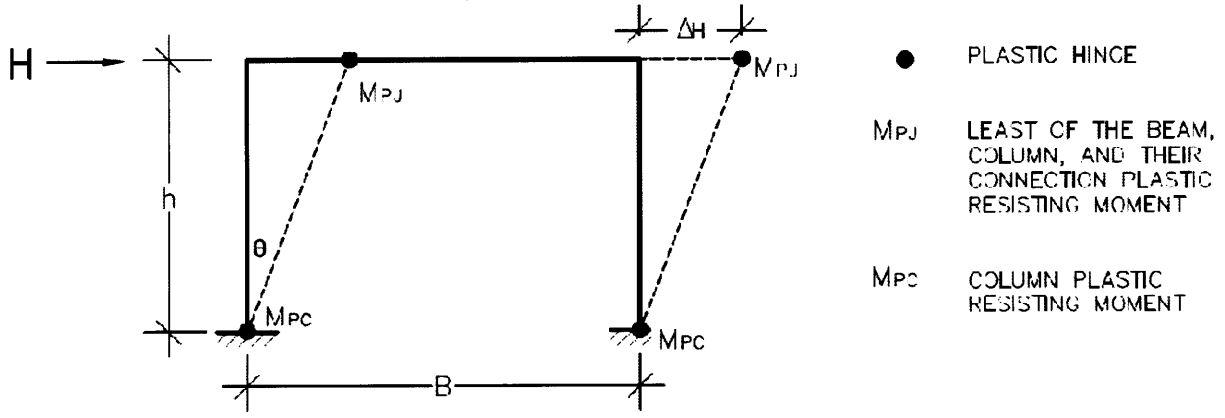

Figure 27: Expected Collapse Mechanism for Single Story Frame under Lateral Load

In this frame, the joint between the beam and the column is a fixed connection, meaning the full bending moment is transmitted at the joint. This is why M_{PJ} is defined as being the lesser of their plastic resisting moment values. Ultimate load can be solved for by the following equations:

$$\sum External\ Work = \sum Internal\ Work$$

$$H_{ULT}\Delta_H = 2M_{PJ}\theta + 2M_{PC}\theta$$

$$H_{ULT} = \frac{2(M_{PJ} + M_{PC})}{h} \qquad \textbf{(Eq. 4-6)}$$

A diagonal is introduced into the model to represent the contribution of the masonry infill, shown in Figure 28. In this model, it is anticipated that plastic hinges will form in the frame at the loaded corners prior to development of the peak load, represented by $M_{PJ,1}$ and $M_{PJ,2}$ in Figure 28 (Saneinejad and Hobbs, 1995). According to research by Saneinejad and Hobbs (1995), the bending moment that has developed at the unloaded corners, represented by $M_{J,1}$ and $M_{J,2}$ in Figure 28, is significantly below the plastic moment value. Therefore, the unloaded corner moments purportedly have negligible effect on the collapse load of the frame. Based on this, their contribution is not included as part of the analysis.

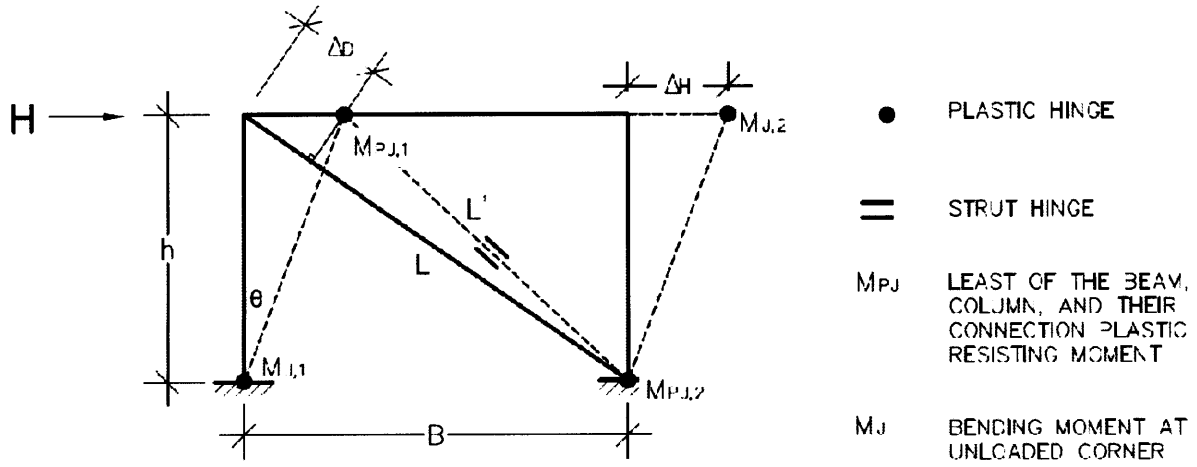

Figure 28: Expected Collapse Mechanism for Single Story Infilled Frame under lateral load

Ultimate load can be solved for by the following equations:

$$\sum External\ Work = \sum Internal\ Work$$

$$H_{ULT}\Delta_H = (M_{PJ,1} + M_{PJ,2})\theta + R_{STRUT}\Delta_D$$

$$H_{ULT} = \frac{(M_{PJ,1} + M_{PJ,2})}{h} + \frac{R_{STRUT}B}{L} \qquad \textbf{(Eq. 4-7)}$$

This general theory can be applied to multi-story and multi-bay frames. As shown in Figure 29(a), a multi-story infilled frame will develop a simple plastic collapse mechanism with plastic hinges only at the loaded corners. This is due to the fact that the unloaded corners of a panel correspond to the loaded corners of the two other panels in the frame (Saneinejad and Hobbs, 1995).

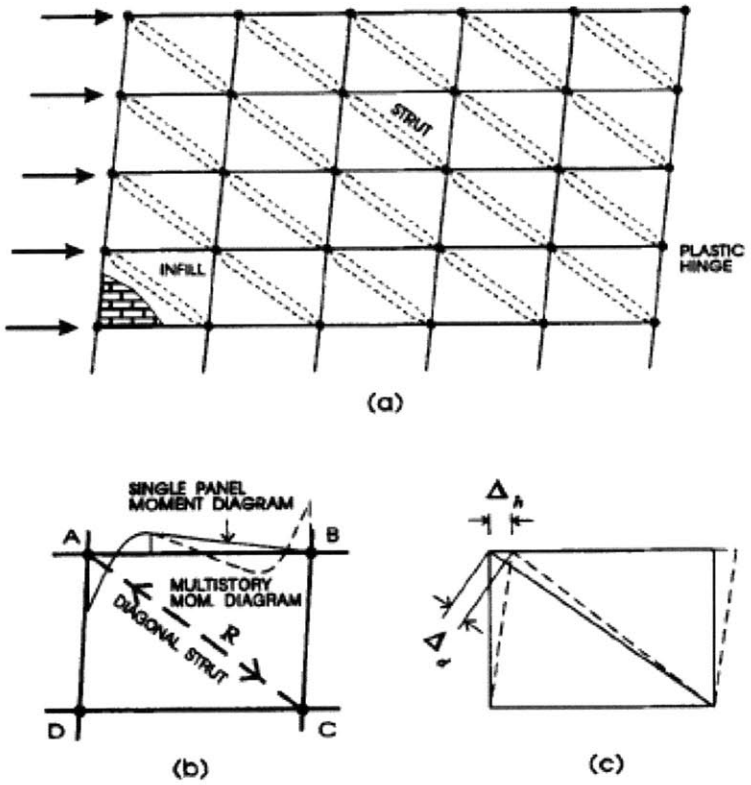

Figure 29: Multi-story Infilled Frame: (a) Mode of Distortion at Peak Load; (b) Moment Distribution; (c) Deflection
Source: Saneinejad and Hobbs, 1995

As shown in Figure 29(b), the bending moment diagram of a multi-story frame does not differ from a single panel in the loaded corner, but there is a significant change in bending moment value in the right-hand side of the beam (point '*B*' in the Figure). However, this is accounted for when considering the upper story panel. Therefore, the infill behavior of a single and multi-story frame are similar and the ultimate load value derived for the isolated panel can also be applied to the multi-story frame (Saneinejad and Hobbs, 1995). With this relationship, the ultimate load on each story of an infilled frame can be calculated and verified that the strength does not exceed expected story shear.

This method is applied to the case study bay. For the case study, it is assumed that failure will occur at the second story because of the large accumulated shear forces and geometric irregularity. Unlike the

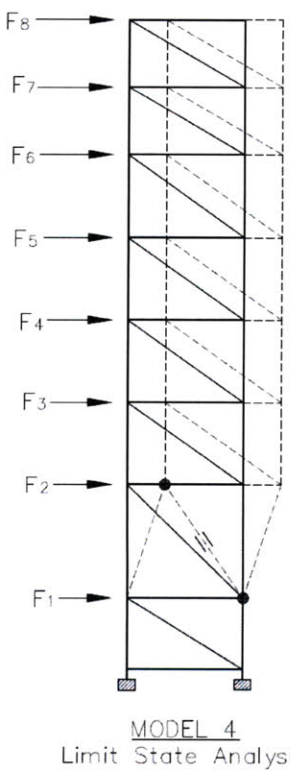

frames introduced above, the case study frame has partial fixity at the beam-column connection. This means that M_{PJ} cannot be defined as the lesser of the beam, column, and connection plastic resisting values. Because the partially fixed connection is not able to transmit significant loads, the bending moment value in the beam will likely be lower than the bending moment value of the column. Therefore, the plastic moment of the column was taken in the calculation. The failure value was calculated using Equation 4.7. Full calculations can be found in Appendix D.

$$H_{ULT} = \frac{(M_{PJ,1} + M_{PJ,2})}{h} + \frac{R_{STRUT} B}{L}$$

$$H_{ULT} = 282\ kips$$

Figure 30: Limit State Analysis Model

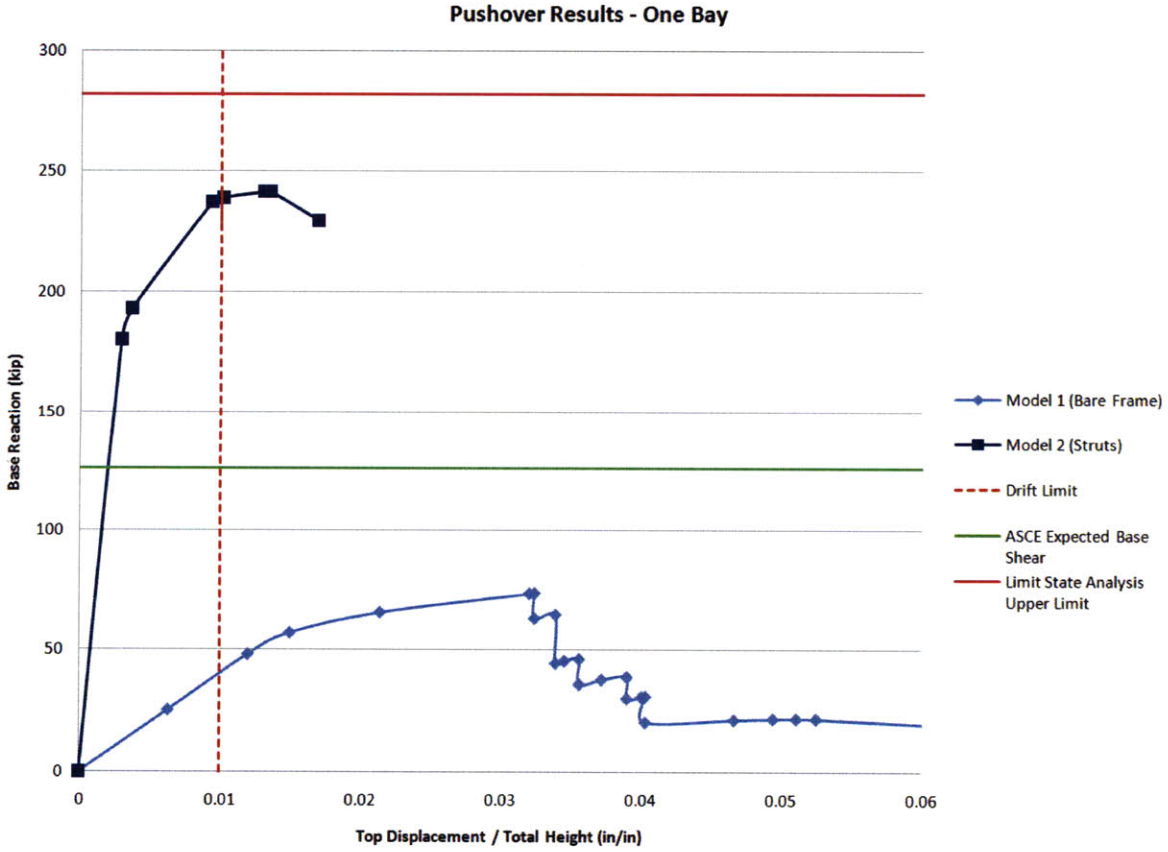

Figure 31: Pushover Curve for Typical Bay with Limit State Analysis Model

This ultimate load found was plotted in the pushover curve, represented by the pink line shown in Figure 31, in order to compare it to the other models. The ultimate load predicted by the limit state analysis was higher than the ultimate load predicted by the finite element model on the order of approximately ten percent. Therefore, it is clear that the simple method outlined about could not be used for an in-depth analysis of an infilled frame structure. However, this value is close enough to the 'actual' ultimate load to be considered useful considering it was accomplished with a relatively simple hand calculation. Overall it is a good method for first-order approximation in order to gain insight into the behavior of the masonry infilled frame.

4.5 Analysis of Full Elevation

Another pushover analysis was performed on a bare frame model of the full elevation (Model A), compared with a full elevation with diagonal struts to represent the masonry infill (Model B), shown in Figure 35.

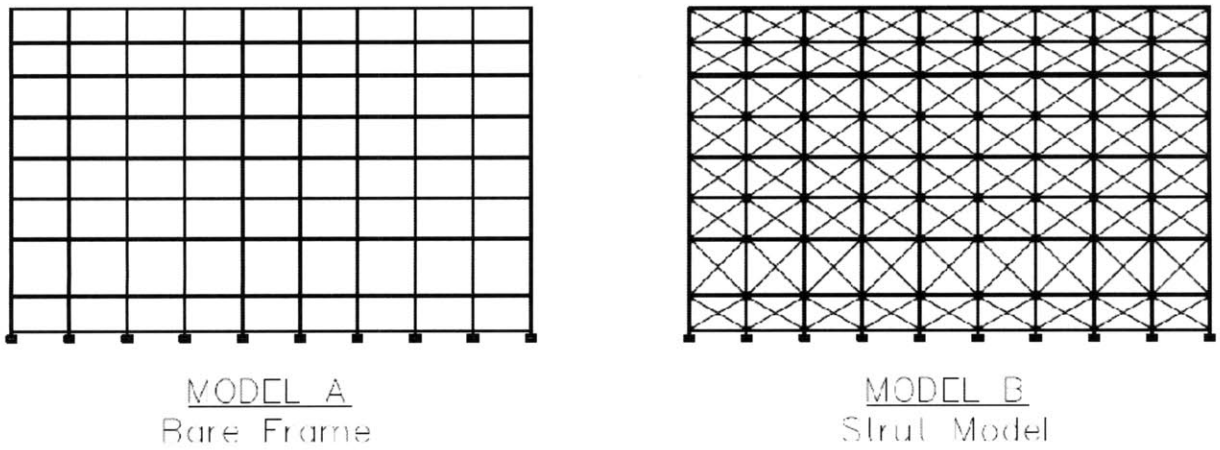

Figure 32: Full Elevation Strut Models

The purpose of this model was to compare it to a limit state analysis performed on a full elevation, shown in Figure 33. The failure value was calculated using Equation 4.7, considering an elevation rather than a single bay. Full calculations can be found in Appendix D.

$$H_{ULT} = \frac{18(M_{PJ,1} + M_{PJ,2})}{h} + \frac{9(R_{STRUT}B)}{L}$$

$$H_{ULT} = 2530\ kips$$

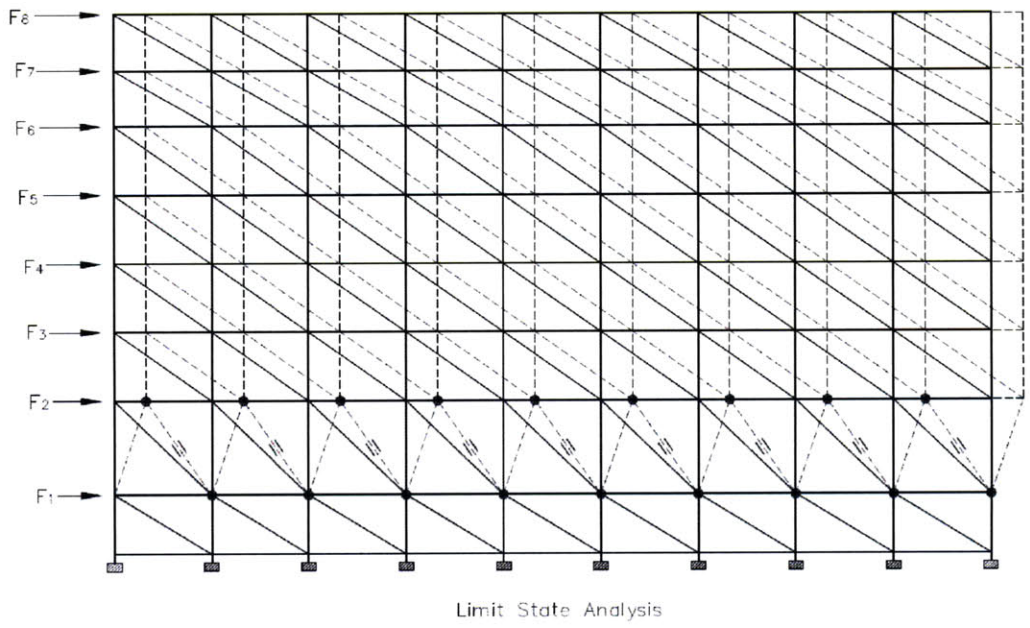

Figure 33: Limit State Analysis of Full Elevation

The results of the limit state analysis compared to the pushover analysis are presented in Figure 34.

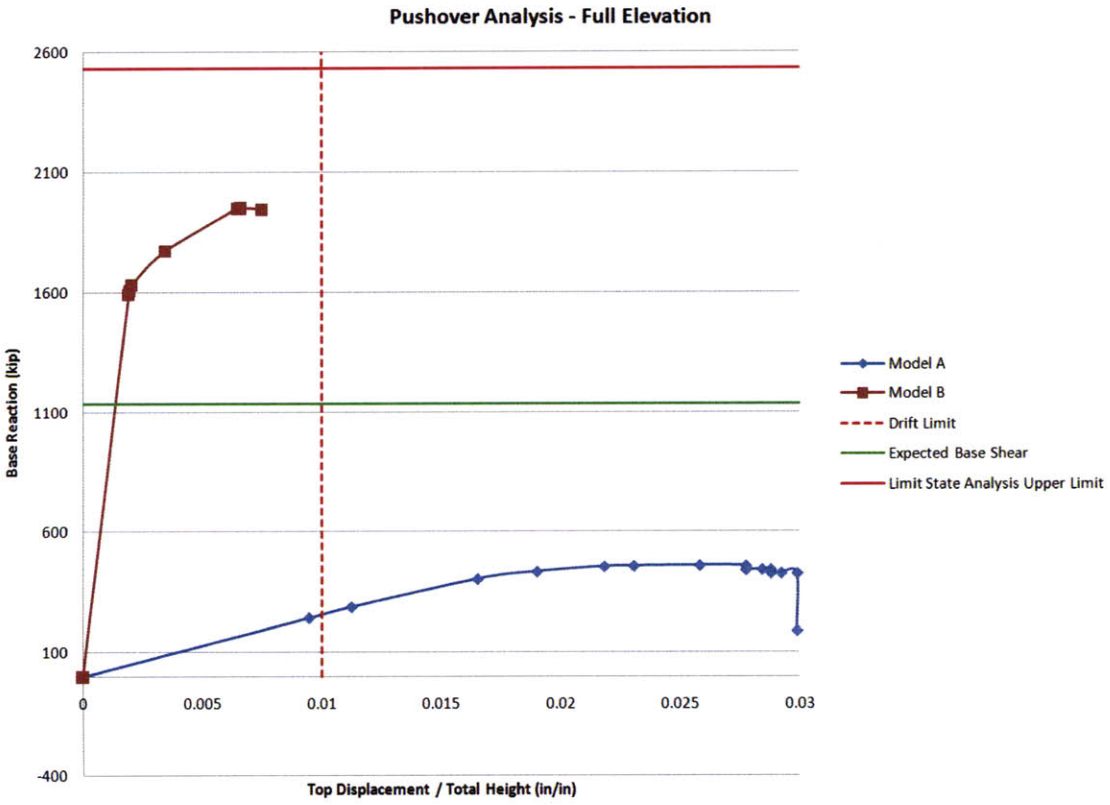

Figure 34: Full Elevation Pushover Analysis

As Figure 34 shows, the value estimated by the limit state analysis is approximately twenty percent higher than what was estimated by the pushover analysis. Potentially, some accuracy was lost as a result of increasing the number of bays. It also might be due to the fact that in reality the beams failed before the columns, which would result in a lower plastic moment value due to their smaller moment of inertia.

4.6 Parametric Study of Different Elevations

Various full elevation model of the prototype building were constructed with different masonry infill configurations, shown in Figure 35.

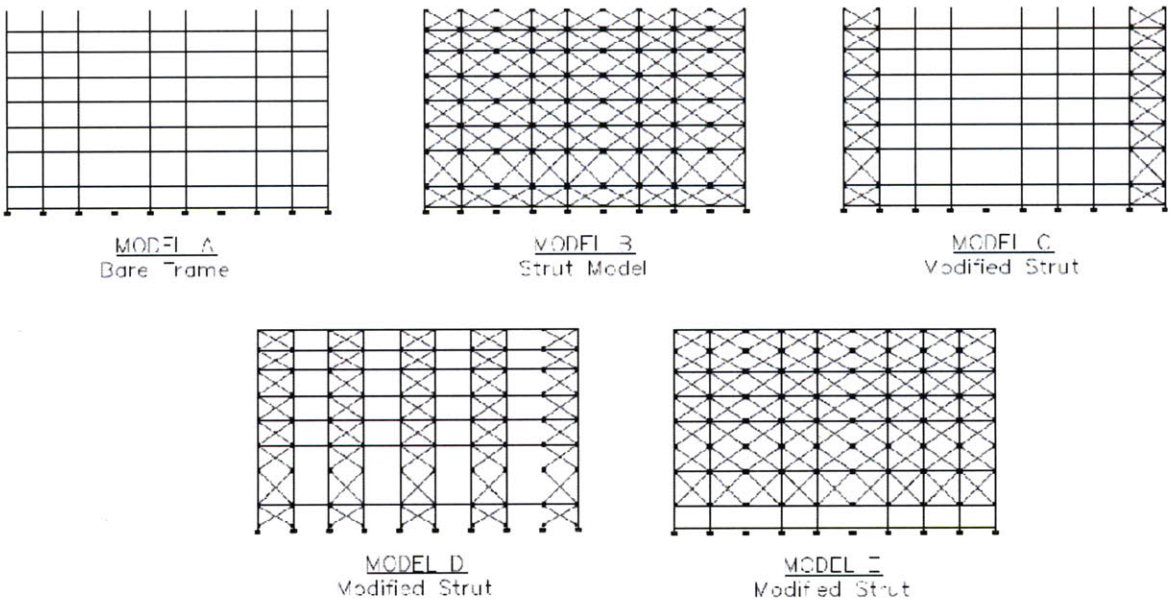

Figure 35: Full Elevation Models

Typically, contribution from masonry infill does not occur along the full length of a building's elevation because of wall openings (windows, doors, storefronts, etc.). However, even if only some of the panels have masonry infill, their presence can still significantly alter the strength, period, ductility, and earthquake performance of the structure. ASCE-41 allows for a diagonally concentric equivalent struts to represent perforated infill panels in lieu of completely neglecting the contribution of panels with openings. However, this was not explored under the scope of this work. Different configurations of infill were tested to see how they affect the structural capacity. Pushover analysis results for the models are presented in Figure 36. Linear elastic and collapse limit forces for each structure are shown in Table 5; failure is indicated by the red cells.

	Model	Base Shear Force (kips)	
		Linear Behavior Limits	Collapse Limits
Bare Frame	A	400	456
Diagonal Struts	B	1600	1950
Modified Strut	C	375	750
Modified Strut	D	910	1235
Modified Strut	E	975	1500
Expected Base Shear (ASCE)		**1135**	

Table 5: Elevation Pushover Analysis Results

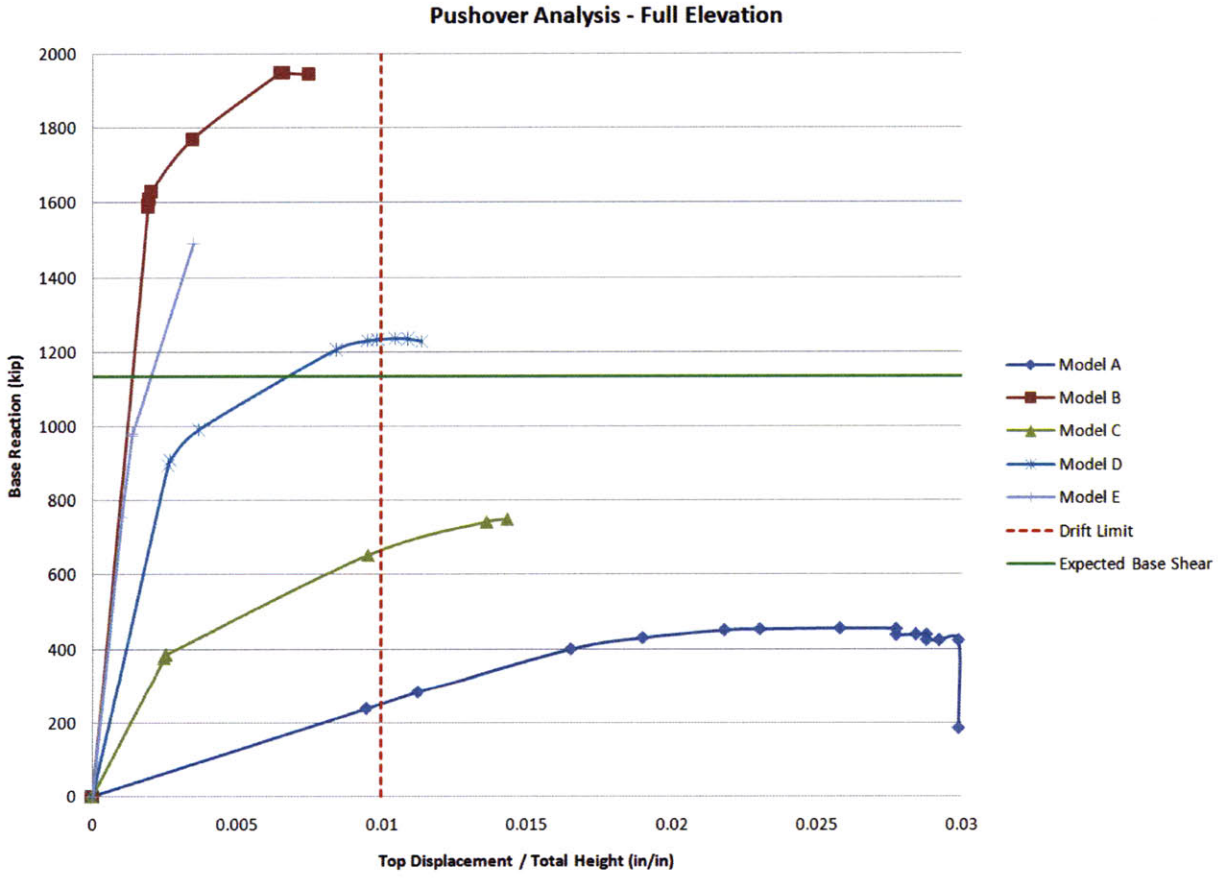

Figure 36: Full Elevation Pushover Analysis

For the most part, models with more masonry infill can withstand higher lateral loads while maintaining lower displacements. However, only Models B, D, and E have sufficient capacity to withstand the expected base shear, indicated in the graph by the green line. Model E, which incorporated a "soft story" at the first level of the building to represent storefront openings, initially acted linearly in a similar

fashion to the fully infilled elevation (Model B). In this case, the stiffness of the masonry infill attracted large shear loads which the steel semi-rigid moment connections in the first story could not handle after initial rotations. This is the only model with infill tested where the steel failed before the masonry, for apparent reasons. In this model, collapse was sudden with limited deflection before failure, as can be seen in Figure 36, which is dangerous from a life safety perspective. Each model in its collapsed state can be seen in Figure 37.

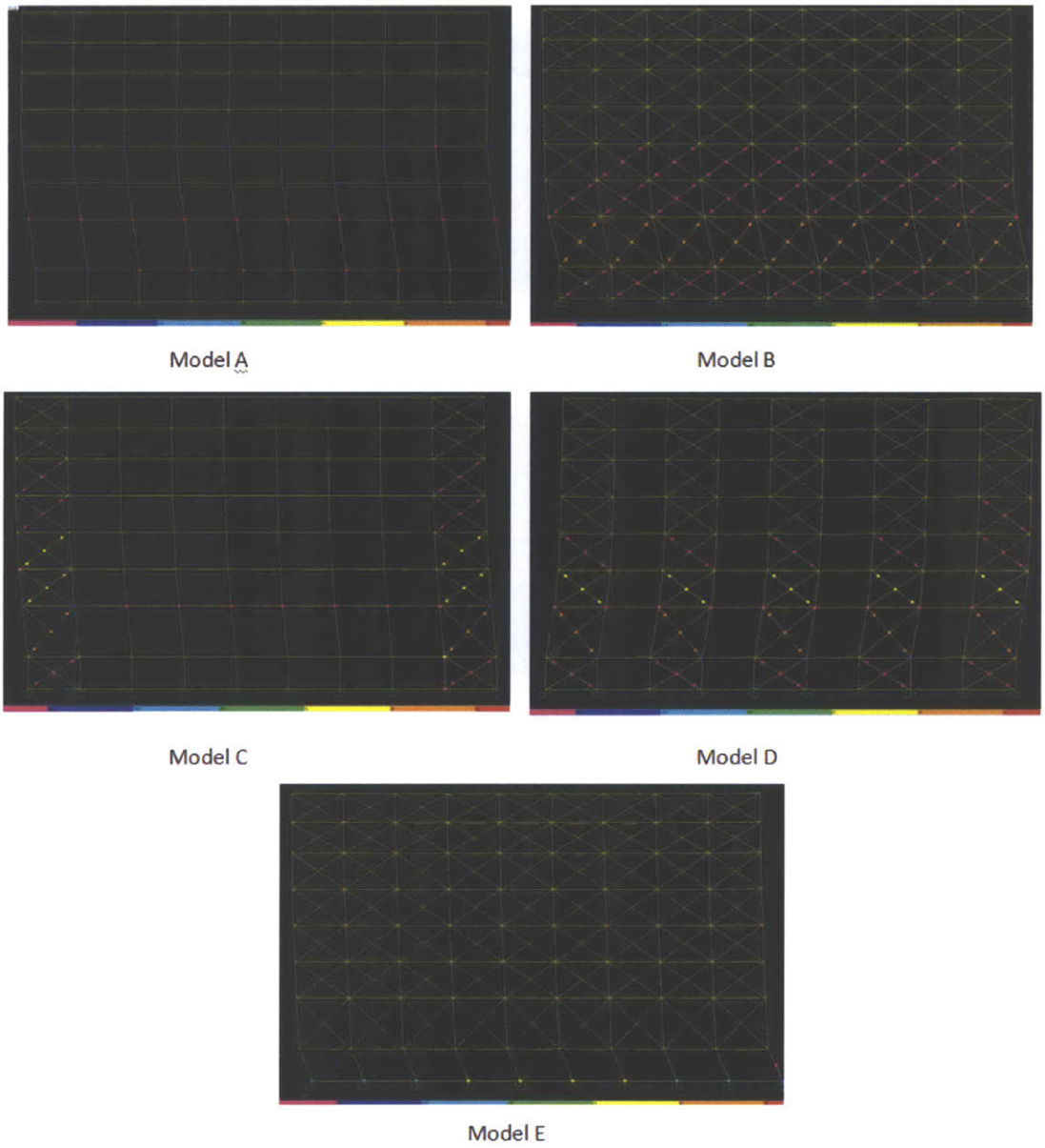

Figure 37: Failure Modes of Different Models

4.7 Conclusion

This Chapter has shown that masonry infill walls have a very important effect on the strength of the building and cannot be considered nonstructural. Main conclusions from the analysis are summarized as follows:

1. The diagonal strut model provides a fairly accurate prediction of structural stiffness and fundamental frequency of masonry infilled frames.
2. Masonry infilled frames can withstand larger base shears while limiting total story drift when compared to a bare frame.
3. At lower stories, the stiffer masonry components will absorb the majority of the lateral load until they are stressed beyond capacity, at which point the frame began to participate in load resistance. Plastic hinges in the steel frame will form before masonry yields in upper stories due to lower shear values at the upper levels.
4. The large height-to-width ratio of the second story made it the most susceptible to failure. In most models, the first plastic hinges formed at the second story because of this geometric discontinuity and because shear force at this level is only slightly less than base shear.
5. The cantilever beam model and limit state analysis are useful ways to estimate the displacement or ultimate force of the masonry infill and can provide accurate results if proper assumptions are made.
6. A masonry infilled structure with a soft first story is susceptible to sudden failure due to high base shear attracted by the masonry that has to be absorbed by the weaker first story frame.
7. Structures with frames that are only partially infilled with masonry can still have considerably higher strength than the bare frame, but how much strength depends on the number and location of the panels.

Although it is a very powerful computational tool, the nonlinear static procedure specified in ASCE-41 does have some limitations. It could be inaccurate if the assumed load distribution is incorrect. The assumed force distribution is based on the fundamental mode which could be misleading if higher modes are significant. In addition, the constructed models do not account for shear effects on beams and columns due to impact from the masonry infill. ASCE-41 requires that these effects are verified as part of the analysis, which was not performed under the scope of this text. However, overall the pushover analysis provides the designer with useful information regarding the capacity and earthquake performance of a masonry infilled structure.

5. Energy Performance of Transitional High Rise Case Study

The thermal performance of uninsulated transitional masonry façades is well below modern standards. In retrofits, it is common practice to add insulation to the wall assembly in order to increase its thermal resistance (R-value). This is beneficial for occupant comfort and reducing the heating and cooling load required of mechanical systems. However, it is important to ensure that insulation retrofits will not compromise the durability of the wall system. This is of particular concern for transitional masonry structures where the steel framing members are embedded within the mass masonry. This Chapter will provide background information on the wall dynamics of mass-masonry walls, and then analyze the wall performance of an uninsulated transitional masonry wall compared to an insulated retrofit.

5.1 Background Information

Solid masonry walls without insulation are subject to a significant temperature gradient, shown in Figure 38(a). Solid masonry walls make use of the large storage capacity of the masonry mass to dry out the moisture by diffusion and capillary wicking to the interior in warm weather or the exterior in cold weather (Straube and Schumacher, 2007). In a cold climate it would be optimum to add the insulation layer to the exterior side of the façade, although this is often not an option due to historic preservation restrictions (Goncalves, 2001). Adding insulation to the interior of the wall assembly lowers the temperature gradient across the masonry wall and brings the temperature of the masonry closer to that of the exterior air, shown in Figure 38(b).

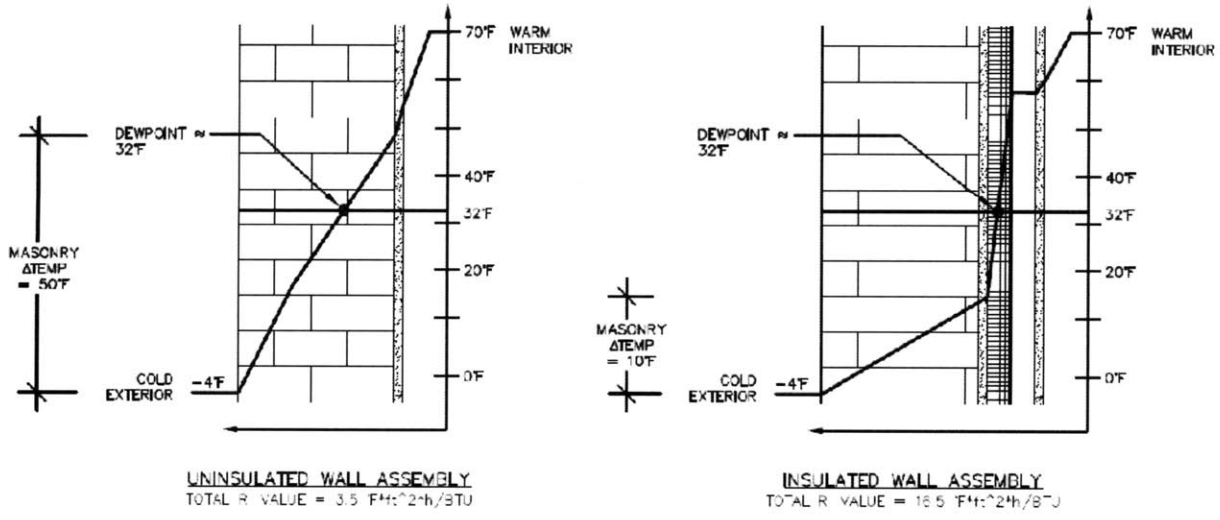

(a) (b)

Figure 38: Vapor Profile of (a) Uninsulated Wall and (b) Insulated Wall Assembly

In cold climates, risks associated with insulation retrofits include increased potential for freeze-thaw deterioration, corrosion of embedded metals, interior plaster finish deterioration, and mold growth. The new insulation results in a reduction of inward drying of the masonry wall. The additional insulation also causes potential for a new wetting mechanism – condensation on the interior face of the masonry due to air leakage, so the new wall assembly should incorporate an airtight layer to the interior of the insulation (Straube and Schumacher, 2007). Certain types of insulation can also act as the airtight layer.

Fiberglass insulation has proven to perform poorly in interior masonry wall retrofits. Among other issues, it is difficult to install achieve proper insulation of the fiberglass flush against the variable masonry wall, creating an air gap where condensation can form. Industry trend has favored the use of semi-permeable foam insulation sprayed directly to the back of the existing masonry wall, with airspace and wall finishes to the interior of the insulation (Straube and Schumacher, 2007). The foam insulation acts as an air barrier as well as an insulator, reducing the potential for condensation on the interior face of the masonry.

5.2 Hygrothermal Simulation

It is necessary to model the dynamics of the proposed renovated wall assembly prior to selecting a retrofit option. Simplified dew-point (Glaser analysis) calculation has proven inaccurately predict of a wall assembly's vapor profile because it only considers steady-state transport under simplified boundary conditions. Preferably, computer software should be used to perform hygrothermal analysis by transient modeling. One such program is WUFI (Wärme und Feuchte instationär). The WUFI program was developed by the Fraunhofer Institute of Building Physics in Germany and is currently being promoted by the Oak Ridge National Laboratory in Tennessee. The program has become an industry standard for vapor drive analysis as it includes the most recent understanding of building physics and employs historic weather patterns for specific project locations. An educational version of WUFI® ORNL 5.0 was utilized for the analysis performed in this Chapter. This noncommercial version of WUFI has the same features as the actual software, but material data could not be manually updated and the calculation period was limited to two years, which sets some limits on the accuracy of the results.

Evaluation Criteria

A model of the existing wall assembly and an insulated retrofit wall assembly were created. Each model is referred to as a "case". The program produces three types of results for each case - water content of

the assembly, relative humidity levels and dew point within the assembly, and the potential for mold growth within the assembly. Each case is examined at each layer of the wall assembly allowing one to view how each individual material is performing.

The main criterion for assessing results is the behavior of the total water content of the assembly. This shows whether or not moisture has accumulated during the investigated period. Reduced drying of the masonry over time could result in freeze-thaw action, as discussed in the previous section. Note that this can vary in different elevations due to environmental factors such as solar gain. There is risk of freeze-thaw action when the temperature within the assembly is below zero and moisture content of the material is above ninety percent (Straube, 2007). Optimum water content performance occurs if there is no accumulation of moisture resulting from vapor drive over the calculation period.

WUFI output provides graphs comparing temperature to relative humidity and dew point. These graphs can be used to determine if there is potential for condensation within the assembly layers and where it may occur. This can be used to determine risk for corrosion of the embedded steel. Corrosion threshold is Time of Wetness, defined by ISO (1992) as hours above 0°C and 80% relative humidity (Straube, 2009).

Wall Assemblies

Figure 39 shows the WUFI model of the existing system. This image shows the face brick (represented by the beige rectangle), followed by alternating layers of mortar joint (grey rectangle) and common brick back-up (maroon rectangle).

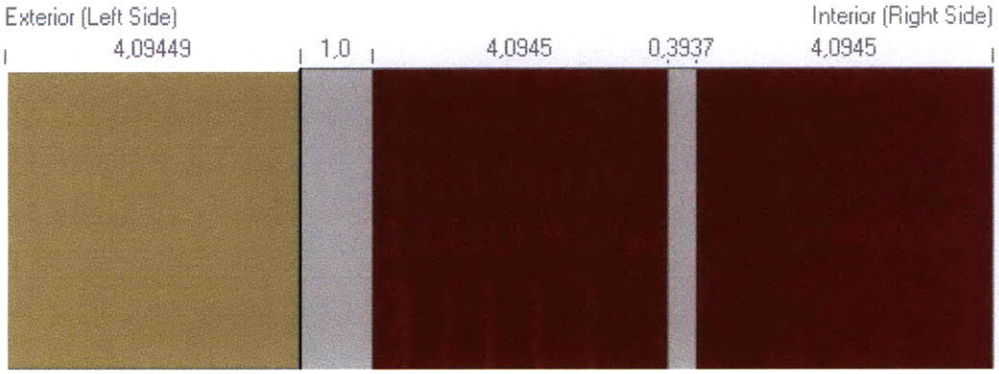

Figure 39: WUFI 5.0 Model of Existing Wall System

The renovated wall assembly will consist of closed-cell semi-permeable spray foam insulation applied directly to the interior face of the brick wall assembly, followed by an air space and interior finishes. This

is shown in Figure 40, where insulation (tan rectangle), air space (cyan rectangle) and interior gypsum sheathing (grey rectangle) have been added to the model. Material properties for both wall assemblies were taken from the WUFI database. As mentioned above, material properties could not be edited in the version of the software used, but in practice it is important to measure and update property values wherever possible.

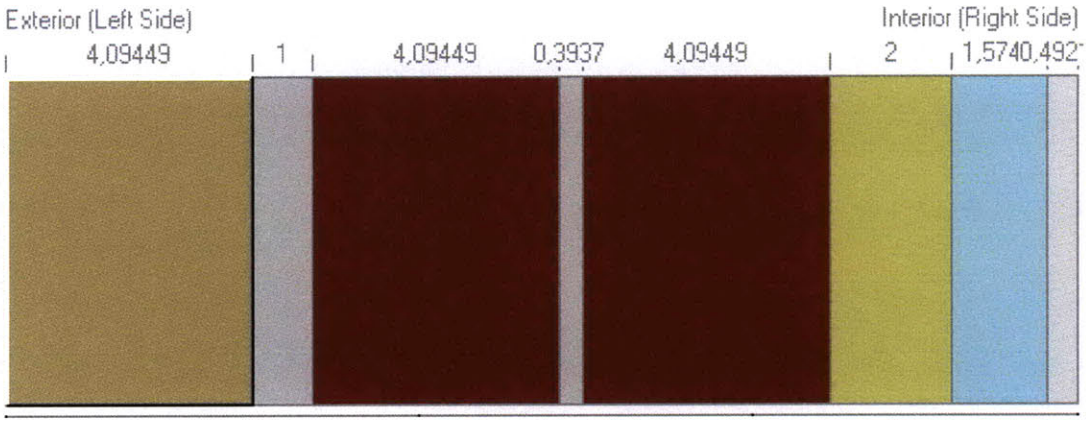

Figure 40: WUFI 5.0 Model of Renovated Wall System

Climate Data

The simulation was run for a two year time period in Boston, Massachusetts. WUFI includes climate data files for most large North America cities, including Boston. Climate data is shown in Figure 41.

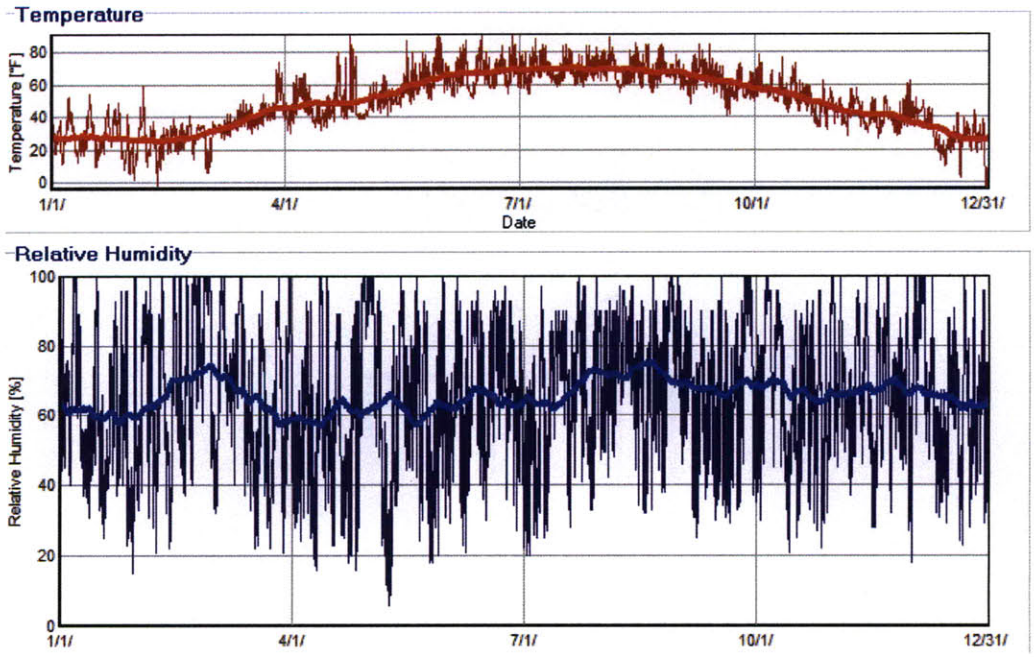

Figure 41: WUFI 5.0 Climate Data for Boston, MA

Results

In terms of total water content, the unrenovated wall assembly performed slightly better than the renovated wall assembly, which showed a slight increase in water content of the overall assembly over the two year calculation period. Further investigation would be necessary to determine if this is of concern – it is possible that the two year calculation period was not long enough for the system to reach the dynamic steady state, and a longer time period should be checked. Of particular interest in a transitional masonry wall assembly is the condition of the wall assembly at the location of the embedded steel, which was assumed to be within the common brick back-up layer. The relative humidity of each wall assembly at the location of the steel is shown in Figure 42 and Figure 43. Potential for corrosion (elevated relative humidity of over 80%) is present in both wall assemblies. However, the relative humidity of the renovated wall assembly remains much closer to 80% throughout all temperature ranges, meaning there is more of a risk of corrosion in the renovated wall assembly.

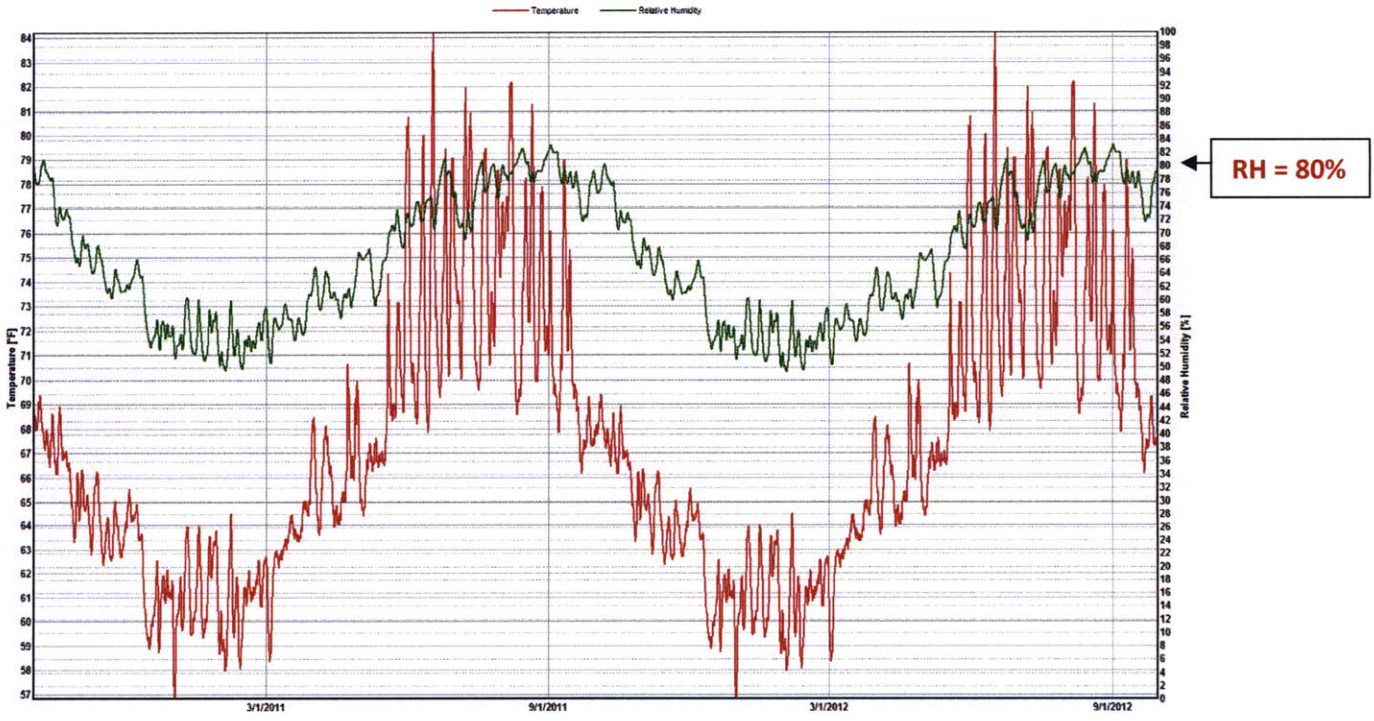

Figure 42: Relative Humidity (Green Line) vs. Time of Unrenovated Wall Assembly at Steel Location

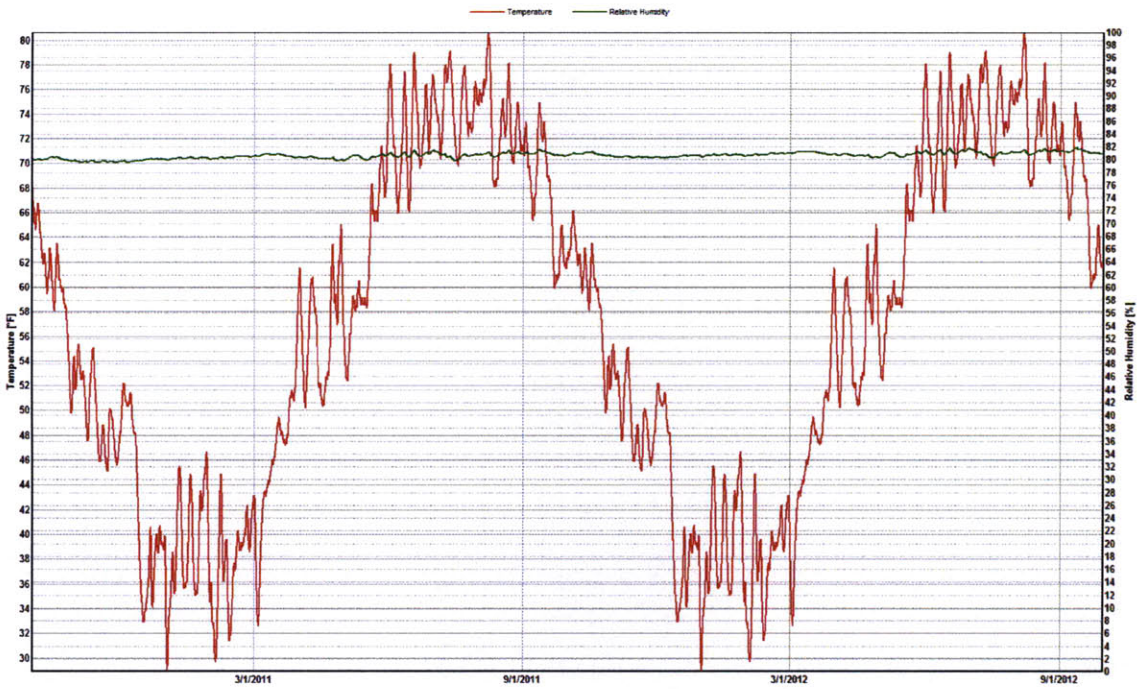

Figure 43: Relative Humidity (Green Line) vs. Time of Renovated Wall Assembly at Steel Location

5.3 Conclusion

Although no industry standards have been adopted, there have been numerous studies done on the effect of adding insulation to multi-wythe masonry wall assemblies. Consensus is that if the dynamics of the wall are properly modeled and considered prior to selecting a retrofit option, it is possible to successfully implement an insulation strategy. However, many studies and experimentation have been done on traditional load bearing masonry walls that do not have a large percentage of embedded steel when compared to transitional masonry façades. It is particularly important in these buildings to ensure that the steel is not put in a humid environment that accelerates corrosion of the structural steel. The restoration community would greatly benefit from additional research, including experimental testing, of the dynamics of transitional masonry walls.

It is also important to consider the limitations of the WUFI software. The program assumes a perfect, continuous wall system with intact building components (i.e. insulation layers are tight together, vapor barriers are continuous, no defects in the external masonry, etc). Additionally, not all the materials provided by the WUFI database are consistent with those used in the United States. It is important to test materials and alter properties to get the most accurate results. Furthermore, the wall that is being retrofitted has been in place for many years, so the measured material values of the unrenovated wall

assembly should be used as the initial values in the model for the assembly to be retrofitted. The modeling software is also one-dimensional, meaning that it does not take into account the impact of structural penetrations or discontinuities when evaluating surface temperatures and heat flow. Software that takes into account two and three-dimensional assemblies, such as WUFI 2D, can better predict response at discontinuities. This type of software models specific details or connections, and as such can check specific spots of concern such as wall penetrations or metal studs.

When considering the retrofit of the wall, it is also important to consider that once the insulation is put into place, particularly if it is a spray-foam type, this is an essentially irreversible process. The insulation cannot be removed without damaging the masonry. It also makes it more difficult to access the embedded steel from the building interior without damaging the insulation. The permanent nature of this retrofit makes it very important that a proper analysis is performed at the beginning of the project.

Lastly, concurrent with the insulation retrofit, it is necessary to make sure that sources of moisture penetration into the wall assembly are reduced, such as from large cracks or defects in the wall assembly, or inadequate ground drainage. An expensive insulation upgrade will be much more effective if sources of moisture penetration are reduced. Air leakage through windows and openings should also be looked at because air leakage is often a significant source of heat loss and occupant discomfort in historic buildings (Goncalves, 2001).

6. Restoration and Retrofit

A firm understanding of the unique nature of transitional masonry buildings is necessary when implementing rehabilitation or retrofit strategies. Restoration scope is project specific and can vary widely depending on an owner's objective. It can be as limited as minimal repairs to comply with façade ordinance requirements or as extensive as a full scale retrofit and seismic upgrade. This Chapter describes procedures for the evaluation of an existing transitional masonry building, issues to consider when specifying façade repairs, and structural retrofit options. Energy considerations are not discussed as this issue was addressed in Chapter 5.

6.1 Building Evaluation

The first step of a restoration project is to obtain all relevant and available information on the building construction, which is compiled through research, field investigation, and testing. The amount of information required is dependent on the project scope, which should be fully defined early on in the project. The scope of the renovation will dictate whether or not the structure has to be brought up to modern code. The bigger the job, the closer the existing building will be expected to be brought to levels of code provisions for new buildings, which includes not only wind and seismic requirements but also thermal performance.

Research

Original construction drawings are one of the most useful sources to determine the structural configuration of an existing building. Unfortunately, in the United States, it is estimated that original drawings exist for less than five percent of historic buildings, with structural analysis records accounting for less than one percent (Rabun, 2000). Renovation drawings from previous work done on the building can provide useful information about building construction. Other sources of background information include the building owner, the local building department, subcontractor shop drawings, old building permits, city or town archives, local libraries, and historical societies.

Field Investigation

The primary source for information is the building itself. In addition to being hard to come by, original drawings may not accurately represent as-built conditions. A visual observation of the structure is the cheapest, easiest, and often the most important way to obtain information about the structural performance. As discussed in Chapter 2, patterns of façade deterioration in transitional masonry facades

are indicative of underlying structural issues. An overview of the building can provide insight into crack patterns, differential movement, if the wall is out of plumb, locations of probable water penetration, and general patterns of wear. For façade evaluations, an inspection of each individual building element and material is necessary to determine its condition. On tall buildings, close-up inspection can be achieved by the installation of scaffolding, swing staging, or industrial rope access techniques. Simple equipment such as binoculars and cameras are sufficient for most evaluations. Moisture meters can be used to determine water content of a material and hammers can be used to sound stone to locate areas of subsurface delamination. More sophisticated equipment, such as 3D laser scanning and photogrammetric cameras can provide dimensioned drawings and images of the façade if hand measurements are not deemed to be accurate enough.

Testing Methods

If information beyond the exterior façade is required, some sort of probe testing is necessary to expose the wall assembly. Destructive testing consists of wholesale removal of specific portions of building assembly in order to expose underlying conditions. Location of destructive tests must be determined by an experienced engineer to ensure that it will provide useful information about underlying components without compromising the structural integrity of the system. Figure 44 shows a destructive test on a transitional masonry façade. Two exterior wythes of masonry were removed to expose the condition of an underlying concrete slab and steel framing member.

Figure 44: Destructive Test Cut of Masonry Façade

Destructive testing is very useful but can be undesirable from a building conservation perspective, particularly if the structure has historic status designation. In addition, the area of the destructive test only encompasses an extremely small percentage of the total building area, so if an irregular condition is randomly exposed it can result in incorrect assumptions about the entire structure.

Nondestructive testing is an alternate method that can either be performed complementary or in lieu of destructive testing. Advanced techniques such as boroscope testing, fiber optics, impulse radar, and acoustical pulse velocity methods can be used in determining the location, composition, and condition of hidden building components. Another technology that is gaining popularity in the renovation community is the use of infrared thermography surveys. Infrared thermography determines temperature differentials at the surface of the material being scanned. By making the thermal radiation of a building visible, this survey aids in determining potential areas of air leakage, moisture infiltration, and energy loss within the assembly. Figure 45 shows an infrared thermogram of an exterior façade that shows heat loss occurring around windows and at each floor level at the concrete slab location, potentially due to thermal bridging.

Figure 45: Infrared Thermogram
Source: Hathaway, 2010

Laboratory testing is also a necessary part of the building evaluation. Crucially, materials must be tested for the presence of asbestos and lead, and potentially polycholorinated biphenyls (PCBs). These elements were commonly used in historic materials such as caulking, sealants, coatings, and paint because of their favorable performance properties before their carcinogenic nature was well known. Specific remediation procedures is necessary for these materials that must be included as part of a project scope. Other laboratory tests that may be performed as part of a building evaluation include chemical and petrographic testing to identify material composition.

6.2 Façade Repair

Repairs to the façade of a transitional masonry building are intended to remediate some of the issues with differential expansion and steel corrosion discussed in Chapter 2. A common way to relieve built-up stress due to differential expansion is to cut horizontal and/or vertical expansion joints into the masonry wall. The mode of deterioration should be properly identified prior to specifying new joints as horizontal and vertical expansion joints serve different purposes. In the case of severely displaced masonry, cutting horizontal expansion joints into the wall to relieve the built-up stress has the potential to be problematic, as the bulged masonry might be unstable from high stress build up. If this condition is suspected, flat-jack testing is recommended to estimate the in-situ stresses in the outer wythe of masonry prior to establishing a repair (Searls and Bronski, 2000).

At corner columns with crack patterns, the most common repair procedure is to remove the masonry, clean and waterproof the underlying steel, and reconstruct the masonry incorporating vertical expansion joints to allow for future differential movement of the perpendicular walls. In some cases it might be necessary to structurally augment severely deteriorated steel members. It is important to note, however, that if vertical expansion joints are introduced at each building corner this will create a weak plane in the corner outer masonry that is not connected to a back-up wall and is totally dependent on the shear and tensile strength of the sealant material. Therefore, it might be necessary to incorporate masonry ties to connect the masonry corner to the back-up structural steel or masonry to ensure that it has adequate out-of-plane stability. A detail of this condition can be seen in Figure 46.

Similarly, removing the exterior wythe of masonry and installing a waterproofing membrane on the face of the back-up wall, in the attempt of mimicking a modern cavity-wall configuration, has the risk of changing the out-of-plane behavior of the wall assembly. The exterior wythe of brick is now acting

primarily as a veneer to transmit load to the back-up wall, and if the back-up common brick/terra-cotta is in poor condition it might not be able to withstand loads without the composite action. The condition of the back-up wall must be assessed to ensure it does not require reinforcement if this type of detail is being adopted.

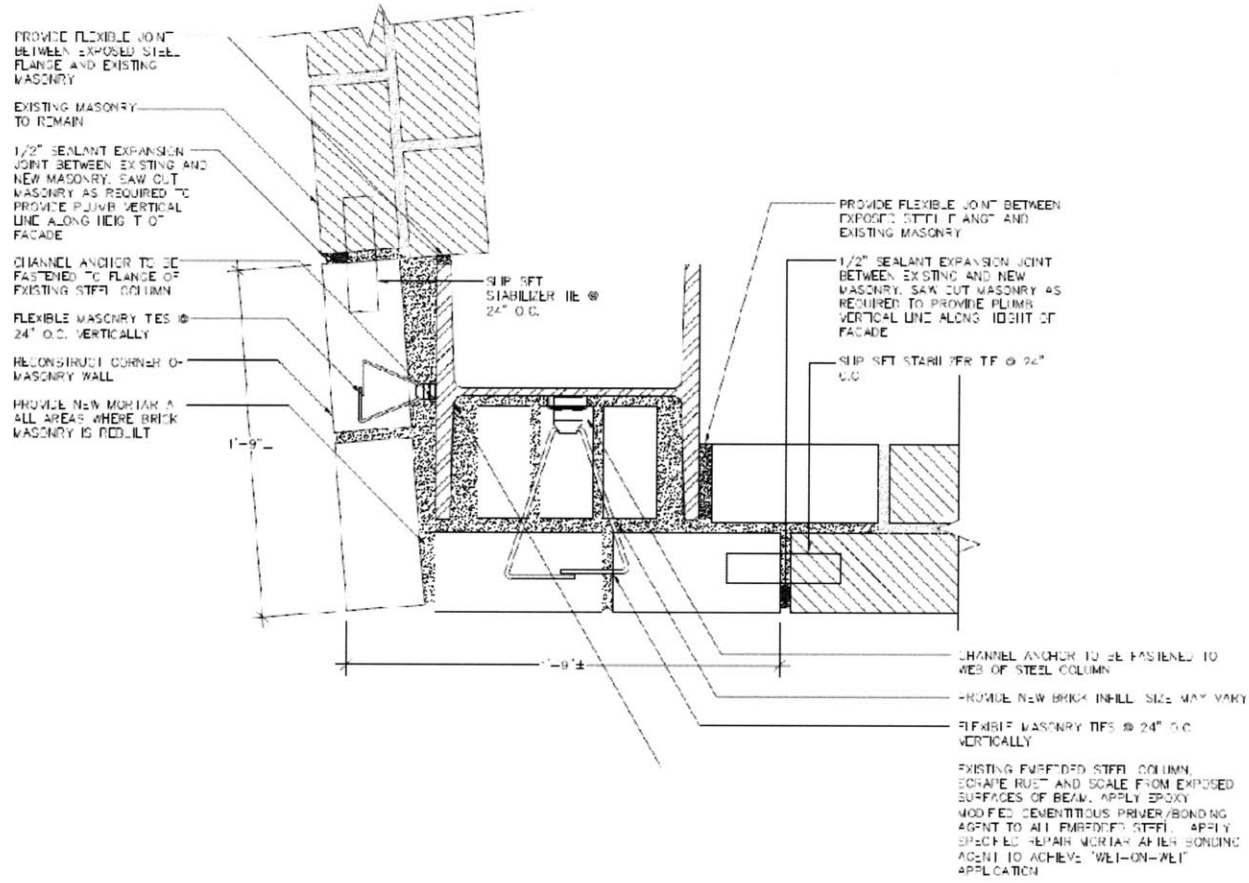

Figure 46: Detail of Masonry Rebuild at Building Corner

Any replacement metal that is introduced into the wall assembly - be it in the form of primary or secondary structural framing, or steel ties/rods - must be galvanized or stainless metal in order to provide durability against moisture penetration.

If repairs are only performed in locations that exhibit rust jacking, this will not address future issues regarding the deterioration of the underlying steel frame. Two practical methods are available for the treatment of steel frame corrosion. The first, described above, is to treat the steel and change its environment by rebuilding sections of a wall assembly. This is often impractical, expensive, and invasive of a historic building façade. An alternate option is to halt the corrosion process electrochemically in the form of cathodic protection. In a simple definition, cathodic protection reverses the direction of the

corrosion current by forcing an ionic current to flow on the steel surface (Gibbs, 1995). Benefits of this process are that much larger areas of steel can be protected for a lower net cost and the façade does not have to be disturbed to perform the process. However, cathodic protection prevents future corrosion but does not address existing deterioration, so if the structure is already in bad condition this will have to be addressed through more destructive methods.

6.3 Structural Retrofit

The first step in the structural retrofit of a transitional masonry façade is to perform a structural analysis that accounts for the nonlinear contribution of the masonry infill in order to determine if it has sufficient capacity to withstand local wind or seismic loading. As previous Chapters have discussed, the contribution of the masonry infill has a great impact on the structural performance of the building. If the analysis indicates that the existing structure has insufficient capacity, then a structural retrofit is in order and different methods will have to be considered based on their feasibility and effectiveness.

The retrofit of masonry infilled structures is a challenge because there are no clearly defined procedures or strategies for the upgrade of these buildings. Traditional retrofitting techniques for infilled frames include epoxy grouting to strengthen the wall, construction of an additional wythe of masonry to increase axial and flexural strength, surface coating with shotcrete and welded wire steel mesh, or post-tensioning of the infill (El-Dakhakhni, 2002). However, many of these methods are labor intensive, highly disruptive of the existing building, and add additional mass to the building attracting even more earthquake loads. More innovative technologies have also been used for the upgrade of masonry infilled frames, including energy dissipating design through the addition of steel frames with viscous dampers or base isolation. Some newer methods of retrofit of masonry infilled structures that are being investigated are intent on increasing the ductility of the masonry infill so that failure in an earthquake setting will not be sudden and brittle. Such methods include the addition of carbon fiber or the installation of a cement based-composite on the face of the infill wall (Shing, 2009). It would be most beneficial to be able to continue to utilize the contribution of the masonry infill to the lateral strength of the building even after the retrofit. Another option to consider is to construct a back-up system, which will absorb loading only if and when the masonry infill has failed. Ideally, the retrofit system should provide additional ductility to bring the structure into conformance with the design code, rather than attempting to change the force level required for the onset of collapse (Langenbach and Kelley, 1991).

7. Conclusion

The intent of this thesis was to provide the reader with a better understanding of the structural and building envelope performance of transitional masonry structures and present the different methods available for their analysis. This thesis has shown how the interaction of the structural frame and masonry in these unique structures impacts the performance of the façade as well as the global structural performance on a whole, and how this is important to consider when performing a retrofit.

7.1 Limitations of the Results

The case study performed in this analysis was located in Boston, Massachusetts, which is a moderate seismic region. Although the lateral load contribution in the structure in this location is important, it might have been better to look at a more severe earthquake risk area such as California. For instance, following the Loma Prieta Earthquake in San Francisco in 1989, the most significant damage was to transitional masonry mid-rise buildings constructed in the early twentieth century (Langenbach and Kelley, 1991). It would also have been interesting to see how well the cantilever beam and limit state analysis methods would have worked for a higher level of force design.

The cantilever beam model proved good stiffness prediction results for a single bay. This model should have been further explored to see how its feasibility and accuracy changes based on different height-to-width dimensions. Also, the height of the structure analyzed was limited to one hundred and twenty feet. During the time period of interest (early 20th century), this would be considered a high rise building but it is a medium-rise structure by modern standards. Further studies could be performed on taller transitional masonry buildings in order to gauge their vulnerability to earthquake loading as well as how this impacts failure modes. The case study only considered two-dimensional frames, which is a reasonable approximation of a full three-dimensional structure if the building is symmetric with negligible torsional effects. In reality, most buildings are not symmetric and will have higher concentrations of masonry infill on less visible facades while front facades typically have larger window or storefront openings. Considering a less ideal structure would have provided more realistic and useful results.

For all analysis, the panels were either treated as fully infilled or not at all. However, various different equivalent strut models have been developed to represent the reduced contribution of infill perforations. ASCE-41 provides a multiple-compression strut model for infills with openings. For further

study and accurate modeling of these buildings, openings should be modeled in this fashion to provide a more accurate representation of the assembly and wall performance. Finally, the analysis presented in this study concentrated on the CC failure mode, which is the most likely failure mode to occur for steel framed infill structures. However, further study should look at the other failure modes and how they would impact the structure.

7.2 Areas of Further Research

For a future study, it would be meaningful to compare the analysis methods studied in this thesis to results from an actual infilled steel frame that has been experimentally tested. In particular, it would be interesting to further explore the capabilities of the limit state analysis method, which has shown to provide useful upper bound approximations. Comparing predicted values to actual experimental results would provide more insight into how accurate these methods really are and allow for the development of a more accurate simplified model.

In general, continued research on structural analysis methods of transitional masonry buildings is necessary. As has been mentioned throughout the paper, there is a global need for simplified methods to predict the performance of these buildings so that the structural contribution of these structures can be accounted for in design. Although in a research setting it is possible to construct relatively accurate numerical models through advanced techniques such as finite element analysis, this is unrealistic to implement in a workplace setting. Furthermore, if the national code recommends using finite element analysis, guidelines for how to do this should be published so that users can build proper numerical models without having to perform significant amounts of research.

This thesis showed that the modified strut model proposed by ASCE-41 provides a reasonable estimation of the contribution of the masonry and for low level loads simple masonry approximations can be used as a good starting point for analysis. Future research should focus on further iterations and improvement of these simplified models in order to accurately represent the performance of the masonry walls. In addition, the research that is presently being done on structural rehabilitation of masonry infilled frames should begin to be applied to national standards. There is a lack of information available to the practicing engineer on how to implement retrofit techniques on these buildings.

References

ASCE/SEI (2006). *Seismic Rehabilitation of Existing Buildings, ASCE/SEI Standard 41-06.* Reston, VA: ASCE/SEI. Print.

Baker, J. and Heyman, J. (1980). *Plastic Design of Frames.* Cambridge: Cambridge University Press. Print.

Baker, I. (1914). *A Treatise on Masonry Construction Tenth Edition.* New York: John Wiley & Sons. Web. 6 Feb 2010. Available from http://googlebooks.com

Birkmire, W. (1906). *The Planning and Construction of High Office-Buildings.* New York: John Wiley & Sons. Print.

BIA Technical Notes (2006). *Volume Changes – Analysis and Effects of Movements.* Reston, VA: Brick Industry Association. Web. Mar. 23. 2010. Available from http://www.gobrick.com

Boston Public Library Fine Arts Department (1912). *Original drawings of purpose-built Filene's store,* Bin numbers: J2, R3, R4, R45, R57, R61, R64, R82, P114, P130.

CSI (2007) *Sap2000 Advanced, Version 11.0.0: Integrated software for structural analysis and design.* Computers and Structures Inc., Berkeley CA.

Cyclopedia of Architecture, Carpentry, and Building; A General Reference Work – Vol 1. Brunauer Press. Web. 21 April 2010. Available from www.chestofbooks.com

Dam, J. (2006). *Heritage Building Envelope Restoration.* 2006 Symposium on Building Envelope Technology, Washington D.C. Web. 1. Dec. 2009. Available from http://www.rjc.ca

Dawe, J.L. and Seah, C.K. (1989). *Behavior of masonry infilled steel frames.* Canadian Journal of Civil Engineering, 16(6): 865-876.

El-Dakhakhni, W. (2002). *Experimental and Analytical Seismic Evaluation of Concrete Masonry-Infilled Steel Frames Retrofitted using GFRP Laminates.* Doctoral Thesis: Drexel University. Web. 25 Feb. 2010. Available from http://idea.library.drexel.edu/handle/1860/38

El-Dakhakhni, W. et al (2003). *Three-Strut Model for Concrete Masonry-Infilled Steel Frames.* Journal of Structural Engineering, Vol. 129, No. 2, February 1, 2003. Web. April 12 1020. Available from www.asce.org

FEMA (1998). *Evaluation of Earthquake damaged concrete and masonry wall buildings: basic procedures manual. FEMA 306.* Washington, D.C.: Federal Emergency Management Agency. Web. 29 Feb. 2010. Available from http://fema.gov/library

FEMA (2000). *Prestandard and commentary for the seismic rehabilitation of buildings. FEMA 356.* Washington, D.C.: Federal Emergency Management Agency, 2000. Web. 29 Feb. 2010. Available from http://fema.gov/library

Friedman, D. (1995). *Historical Building Construction: Design, Materials, and Technology.* New York: W.W. Norton & Company. Print.

Friedman, D and Oppenheimer, M. (1997). *The Design of Renovations.* New York: W.W. Norton & Company. Print.

Friedman, D. (2005). *Analysis of steel-structure/masonry-wall interaction in historic buildings.* Structural Analysis of Historical Constructions. Possibilities of numerical and experimental techniques. London: Taylor & Francis Group: 103-110. Print.

Friedman, D (2009). *Early Predictions of Steel-Frame Deterioration: Permanency in High-Rise Construction.* Proceedings of the Third International Congress on Construction History, Cottbus, May 2009: 627 – 634. Web. 14 April 2010. Available from https://www-docs.tu-cottbus.de/bautechnikgeschichte/public/openaccess/friedman_oa.pdf

Gibbs, P. (1995). *Cathodic Protection of Early Steel Framed Buildings.* Corrosion Protection Association: CPA Technical Notes No.7. Web. 1 April 2010. Available from www.corrosionprevention.org.uk/

Goncalves, M. (2001). *Insulating Solid Masonry Walls.* Building Envelope Forum. Web. 30 April 2010. Available from http://www.cebq.org/documents/Insulatingsolidmasonrywalls-BEF_000.pdf

Hathaway, O. (2010). *Comparative Analysis of Insulation Methods for Transitional Masonry Structures: A Case Study of Three College Dormitories.* APT Northeast 2010 Annual Meeting and Symposium.

Kidder, F. (1906). *Building Construction and Superintendence. Part I – Mason's Work.* New York: W.T. Comstock. Print.

Kidder, F. (1921). *The Architects' and Builder's Handbook Seventeenth Edition.* New York: John Wiley & Sons, Inc. Web. 1 March 2010. Available from http://googlebooks.com

Knobloch, P. (1931). *Good Practice in Construction.* New York: The Pencil Points Press, Inc. Print.

Holmes, W. (2009). *Evolution of Building Code Seismic Performance Standards for New and Existing Buildings.* Presented at EERI Annual Meeting, Salt Lake City 2009. Web. 21 April 2010. Available from https://www.wsspc.org/Events/2009ac/Holmes.pdf

ICC (2006). 2006 *International Building Code.* International Code Council. Print.

Langenbach, R. and Kelley, J. (1991). *'Soft' Energy Dissipating Design for the Seismic Strengthening of Masonry Infill Frame Midrise Buildings: The Woodrow Hotel, Oakland.* NPS Conference on the Seismic Strengthening of Historic Buildings Proceedings, San Francisco, CA, October 1991. Web. 24 Feb. 2010. Available from www.conservationtech.com

Monadnock Building History (2010). Monadnock Building. Web. 7 April 2010. Available from http://www.monadnockbuilding.com/history.htm

O'Brien, S. (2006). *Walls Still Growing Up.* Architecture Week. Page B1.2. 10 May 2006. Web. 7 April 2010. Available from http://www.architectureweek.com/2006/0510/building_1-2.html

Rabun, J. (2000). *Structural Analysis of Historic Buildings.* New York: John Wiley & Sons, Inc. Print.

Saneinejad, A., and Hobbs, B. (1995). *Inelastic Design of Infilled Frames*. Journal of Structural Engineering, Vol. 121 No. 4, 634–650. Print.

Searls, C. and Bronski, M. (2000). *Early Twentieth Century Transitional Facades in the United States: Common Maladies.* Proceedings of UNESCO-ICOMOS Millennium Congress, Paris, France. Web. 11 Nov. 2009. Available from www.unesco.org/archi2000/pdf/bronski.pdf

Shing, P.B. and Mehrabi A.B. (2002). *Behaviour and Analysis of Masonry-Infilled Frames.* Progress in Structural Engineering and Materials, vol 4, issue 3: 320-331.

Shing, P.B., et al (2009). *Seismic Performance of non-ductile RC frames with brick infill.* ATC/SEI Conference on Improving the Seismic Performance of Existing Buildings and Other Structures, 1117-28.

Straube, J. and Schumacher, C. (2007). *Interior Insulation Retrofits of Load-Bearing Masonry Walls in Cold Climates.* Building Science Digest 114. Building Science Press. Web. 23 Feb. 2010. Available from www.buildingscience.com

Straube, J. (2009). *Measuring the Impact of Interior Insulation on Solid Masonry Walls in a Cold Climate.* Research Report – 0910. Building Science Press. Web. 30 April 2010. Available from www.buildingscience.com

Stockbridge, J. (1983). *The Interaction between exterior walls and building frames in historic tall buildings.* Development in Tall Buildings 1983. Ed. Lynn Beedle. Stroudsburg, PA: Hutchinson Ross Publishing Company: 257-263. Print.

Teeuwen, P.A. (1999). *Lateral Behavior of Steel Frames with Discretely Connected Precast Concrete Infill Panels.* Doctoral Thesis: Eidenhoven University of Technology. Web. 11 April 2009. Available from alexandria.tue.nl/extra2/200613072.pdf

Twelvetrees, W.N. (1900). *Structural Iron and Steel.* New York: Whittaker & Co. Web. 6 Feb. 2010. Available from http://googlebooks.com

Appendix A
Seismic Response Spectrum and Calculations

Seismic Response Calculations

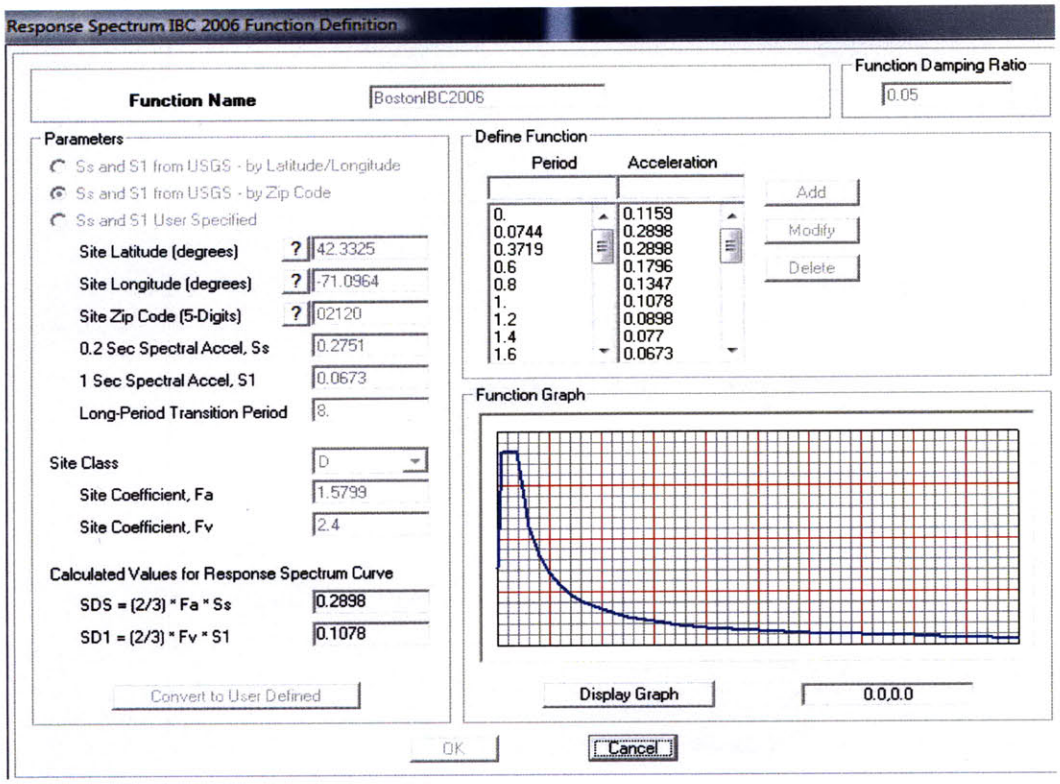

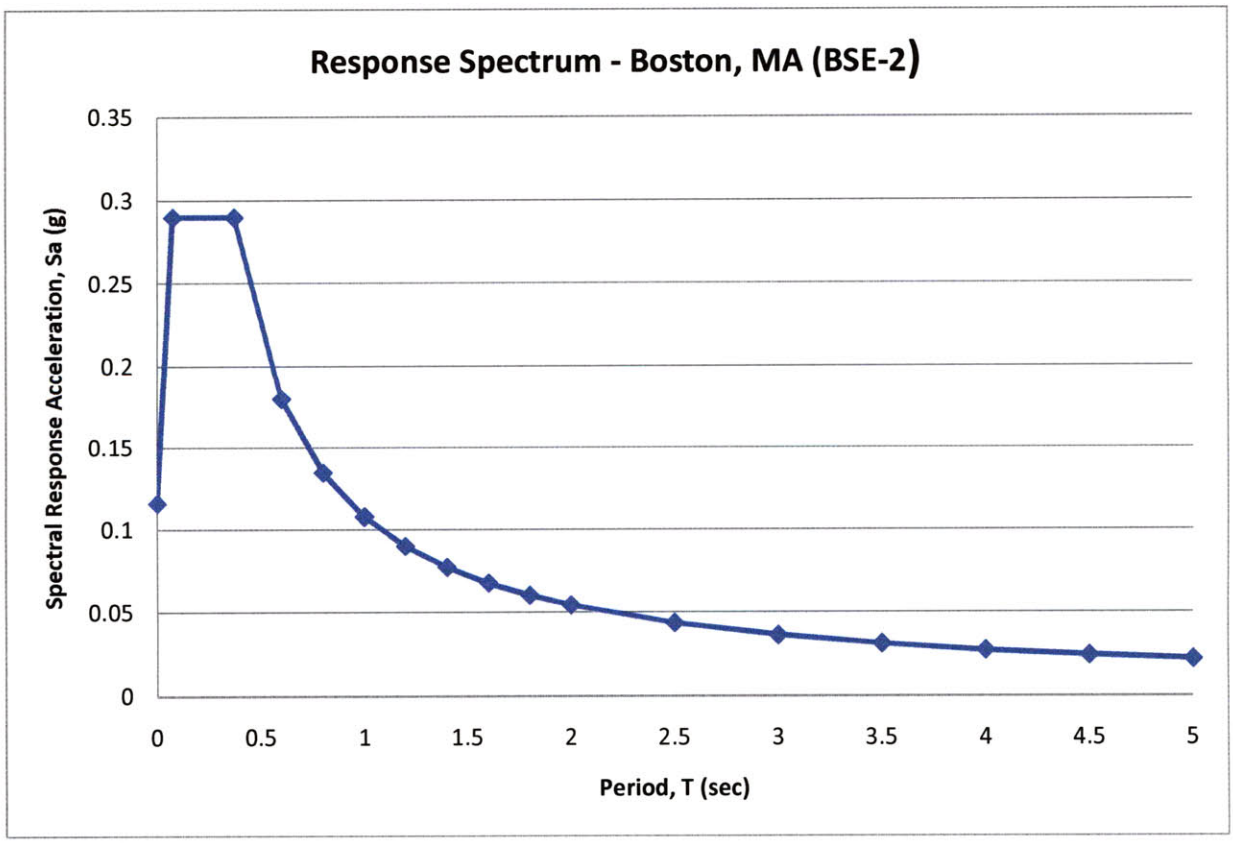

Building Response Calculations

I.Bare Frame

T1 4.05 sec

FROM SAP2000		
S_a	0.04	g
T_e	4.40	sec
g	32.2	ft/sec^2
R	1.24	
C_0	1.5	
C_1	1.000206612	
C_2	1.00	
delta	0.95	ft
	11.37	in
150%	17.06	in

II. Strut Model

T1 0.91 sec

FROM SAP2000		
S_a	0.144	g
T_e	1.13	sec
g	32.2	ft/sec^2
R	0.705	
C_0	1.5	
C_1	1	
C_2	1.00	
delta	0.22	ft
	2.68	in
150%	4.01	in

III. Code Drift Calculations

TABLE 12.12-1 ALLOWABLE STORY DRIFT, Δ_a[a,b]

Structure	Occupancy Category		
	I or II	III	IV
Structures, other than masonry shear wall structures, 4 stories or less with interior walls, partitions, ceilings and exterior wall systems that have been designed to accommodate the story drifts.	$0.025h_{sx}$[c]	$0.020h_{sx}$	$0.015h_{sx}$
Masonry cantilever shear wall structures[d]	$0.010h_{sx}$	$0.010h_{sx}$	$0.010h_{sx}$
Other masonry shear wall structures	$0.007h_{sx}$	$0.007h_{sx}$	$0.007h_{sx}$
All other structures	$0.020h_{sx}$	$0.015h_{sx}$	$0.010h_{sx}$

[a] h_{sx} is the story height below Level x.
[b] For seismic force–resisting systems comprised solely of moment frames in Seismic Design Categories D, E, and F, the allowable story drift shall comply with the requirements of Section 12.12.1.1.
[c] There shall be no drift limit for single-story structures with interior walls, partitions, ceilings, and exterior wall systems that have been designed to accommodate the story drifts. The structure separation requirement of Section 12.12.3 is not waived.
[d] Structures in which the basic structural system consists of masonry shear walls designed as vertical elements cantilevered from their base or foundation support which are so constructed that moment transfer between shear walls (coupling) is negligible.

Delta 1.23 ft

14.76 in

Static Seismic Base Shear and Lateral Force Distribution

ASCE 7-05

Building Information

Lateral System Type	SW		
Number of Stories	9		
Building Height (h_n)	122.33	ft	
Total Weight (W)	50400	kips	
Response Modification Factor (R)	3.25		[ASCE 7-05 Table 12.2-1]
Occupancy Category	II		[ASCE 7-05 Table 1-1]
Importance Factor (I)	1		[ASCE 7-05 Table 11.5-1]
Seismic Design Category	B		[ASCE 7-05 Table 11.6-1]

Site Spectral Data

Mapped MCE spectral response acceleration (S_s)	0.2751	g	
Mapped MCE spectral respone acceleration at T = 1s (S_1)	0.0673	g	
Site Class	D		[ASCE 7-05 11.4]
Site Coefficient F_a	1.4		[ASCE 7-05 Table 11.4-1]
Site Coefficient F_v	2.4		[ASCE 7-05 Table 11.4-2]
MCE spectral response acceleration for short periods (S_{MS}) = F_a*S_s	0.385	g	
MCE spectral response acceleration for 1s (S_{M1}) = F_v*S_1	0.162	g	
Design EQ SRA at short periods (S_{DS}) = 2/3*S_{MS}	0.257	g	
Design EQ SRA at short periods (S_{D1}) = 2/3*S_{M1}	0.108	g	

Building Period

Period parameter Ct	0.02		[ASCE 7-05 Table 12.8-2]
Period parameter x	0.75		[ASCE 7-05 Table 12.8-2]
Period (T_a) = C_t*h_n^x	0.74	sec	[ASEC 7-05 EQ12.8-7]
Long period transition period (T_L)	6	sec	[ASEC 7-05 Figure 22-15 and 22-16]

Base Shear

Seismic Response Factor (C_S) = S_{DS}/(R/I)	0.079	g	
C_{smax} = S_{D1}/(T*R/I) if T<T_L	0.045	g	
C_{smax} = S_{D1}*T_L/(T^2*R/I) if T>T_L	N/A	g	
C_{smin}	0.010	g	[ASCE 7-05 EQ12.8-5]
C_{smin} = 0.5*S_1/(R/I) if S_1>=0.6g	N/A	g	
Governing C_s Factor	0.045	g	
Base Shear (V) = C_s * W	2270	kips	

Vertical Distribution of Lateral Force

Floor Level	Story Weight	Height (ft)	k[1]	w_x*h_x^k	C_{vx} w_x*h_x^k / Σw_i*h_i^k	F_x = C_{vx}*V
8	6300	122.323	1.12	1357764.11	0.2232	507
7	6300	109	1.12	1199551.68	0.1972	448
6	6300	96.66	1.12	1043550.13	0.1715	389
5	6300	81.16	1.12	858350.254	0.1411	320
4	6300	66	1.12	677295.155	0.1113	253
3	6300	50.16	1.12	501250.625	0.0824	187
2	6300	34.66	1.12	331596.912	0.0545	124
1	6300	13.33	1.12	113949.362	0.0187	43

[1] if T<0.5 k=1, if T>2.5 k=2, otherwise k is linearly interpolated between 1 and 2 based on T

Assuming Symmetric Building in Case Study

Base Shear for one Elevation 1135 kips

Base Shear for one Bay 126.1 kips

Appendix B
Masonry Infill Strut Calculations

Masonry InFill Strut Calculations

General Properties		*Item Description*
E_{fe}	30000 ksi	Modulus of elasticity of steel frame material (Friedman, pg 178)
f'_{m_90}	1170 psi	Compressive strength of brick ⊥ bed joint (ASCE 41 Table 7-1 and 7-2)
E_{me_90}	900900 psi	Young's modulus of brick ⊥ bed joint = $700f'_{m\_90}$ (ACI 530 1.8.2.2.1)
f'_{m_0}	819 psi	Strength of brick ll bed joint ($.7f'_{m\_90}$ Seah, 1998)
E_{me_0}	566943 psi	Young's modulus of brick ll bed joint , Ey=Ex/(1+2pi*f) (Lu, 2006)
G	360360 psi	Shear Modulus=$.4E_{me\_90}$ (ASCE 41 7.2.2.7)
v_{0_90}	0.2	Poisson's ratio for masonry (Seah, 1999)
L_{inf}	264 in	Length of infill panel
t_{inf}	12 in	Thickness of masonry infill, composite properties

Floor	**1**	MH-1
h_{col}	160.00 in	
h_{inf}	159.32 in	
r_{inf}	308.35 in	
θ	0.54 rad	
Column	W14x342	
I_c	4900 in^4	
Beam	W14x257	
depth	16.38 in	
λ_1	0.10	ASCE 41, Equation 7-7
a	1.48 ft	ASCE 41, Equation 7-7
A	213.16 in^2	

Stress-Strain Curve

E_{me_θ}	698381 psi	(El-Dakhakhni, 2003, Eqn 10)
f'_{m_θ}	998 psi	E_{me_θ}/700 (El-Dakhakhni, 2003, Eqn 10)
E_p	349190 psi	$E_p=.5E_{me\_\theta}$ (El-Dakhakhni, 2003)
ε_p	0.002857143	
ε_1	0.001857143	ε_p - .001
ε_2	0.003857143	ε_p + .001
ε_u	0.01	

x (ε)	y (σ)
0	0
0.001857	998
0.002857	998
0.003857	998
0.01	0

x (δ, in)	y (F, kip)
0	0
0.572645	212.67
0.880992	212.67
1.18934	212.67
3.083473	0

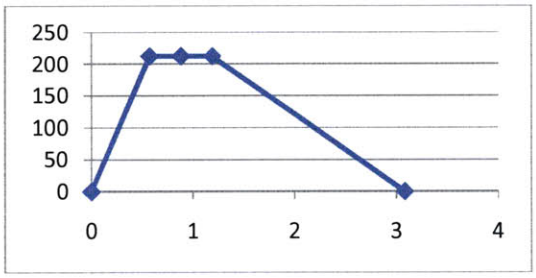

Floor	2		MH-2
h_{col}	256.00	in	
h_{inf}	246.50	in	
r_{inf}	361.19	in	
θ	0.75	rad	
Column	W14x311		
I_c	4300	in^4	
Beam	W14x176		
depth	15.22	in	

λ_1	0.10	ASCE 41, Equation 7-7
a	1.46 ft	ASCE 41, Equation 7-7
A	210.78 in^2	

Stress-Strain Curve

E_{me_θ}	794185 psi	(El-Dakhakhni, 2003, Eqn 10)	
f'_{m_θ}	1135 psi	E_{me_θ}/700 (El-Dakhakhni, 2003, Eqn 10)	
E_p	397093 psi	E_p=.5E_{me_θ} (El-Dakhakhni, 2003)	
ε_p	0.002857143		
ε_1	0.001857143	ε_p - .001	
ε_2	0.003857143	ε_p + .001	
ε_u	0.01		

x (ε)	y (σ)
0	0
0.001857	1135
0.002857	1135
0.003857	1135
0.01	0

x (δ, in)	y (F, kip)
0	0
0.572645	241.84
0.880992	241.84
1.18934	241.84
3.083473	0

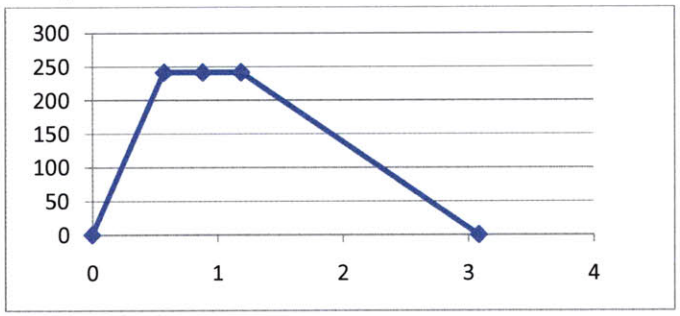

Floor	3 through 6		MH-3
h_{col}	186	in	
h_{inf}	164.58	in	
r_{inf}	311.10	in	
θ	0.56	rad	
Column	W14x257		
I_c	3400	in^4	
Beam	W14x176		
depth	15.22	in	

λ_1	0.11	ASCE 41, Equation 7-7
a	1.36 ft	ASCE 41, Equation 7-7
A	195.57 in^2	

Stress-Strain Curve

E_{me_θ}	704850	psi	(El-Dakhakhni, 2003, Eqn 10)	**x (ε)**	**y (σ)**
f'_{m_θ}	1007	psi	E_{me_θ}/700 (El-Dakhakhni, 2003, Eqn 10)	0	0
E_p	352425	psi	E_p=.5E_{me_θ} (El-Dakhakhni, 2003)	0.001857	1007
ε_p	0.002857143			0.002857	1007
ε_1	0.001857143		ε_p - .001	0.003857	1007
ε_2	0.003857143		ε_p + .001	0.01	0
ε_u	0.01				

x (δ, in)	**y (F, kip)**
0	0
0.572645	214.64
0.880992	214.64
1.18934	214.64
3.083473	0

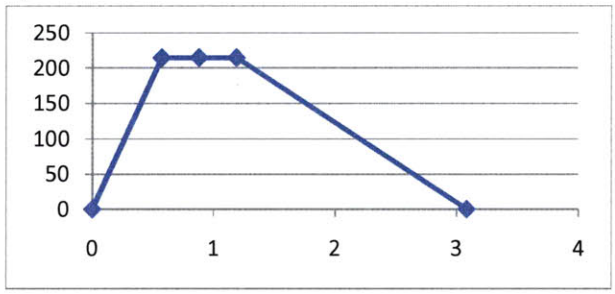

Floor	**7 through**	**8**	MH-4

h_{col}	154.00	in	
h_{inf}	134.85	in	
r_{inf}	296.44	in	
θ	0.47	rad	
Column	W14x257	in^4	
I_c	3400		
Beam	W14x176		
depth	15.22	in	
λ_1	0.11		ASCE 41, Equation 7-7
a	1.38	ft	ASCE 41, Equation 7-7
A	199.05	in^2	

Stress-Strain Curve

E_{me_θ}	668199	psi	(El-Dakhakhni, 2003, Eqn 10)	**x (ε)**	**y (σ)**
f'_{m_θ}	955	psi	E_{me_θ}/700 (El-Dakhakhni, 2003, Eqn 10)	0	0
E_p	334100	psi	E_p=.5E_{me_θ} (El-Dakhakhni, 2003)	0.001857	955
ε_p	0.002857143			0.002857	955
ε_1	0.001857143		ε_p - .001	0.003857	955
ε_2	0.003857143		ε_p + .001	0.01	0
ε_u	0.01				

x (δ, in)	**y (F, kip)**
0	0
0.572645	203.48
0.880992	203.48
1.18934	203.48
3.083473	0

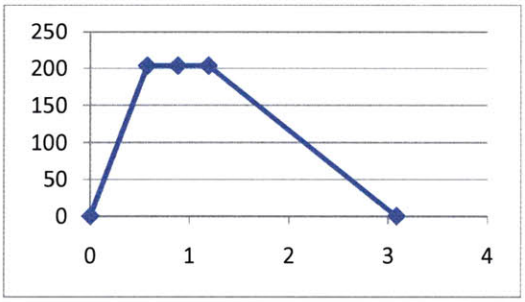

Appendix C
Cantilever Beam Calculations

Calculate Displacement of Shear Beam as a function of height @ node A

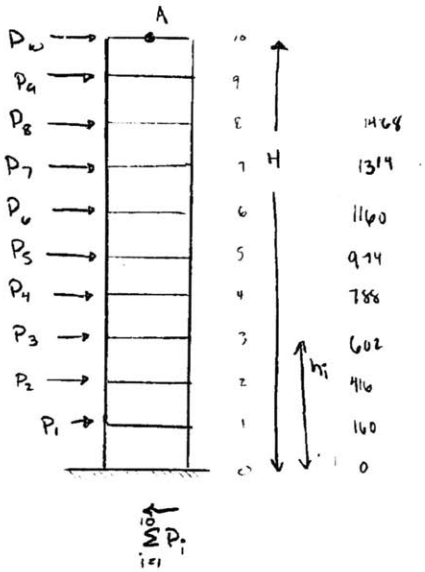

Force P1

$$M(x) = P_1(h_1 - x) \qquad 0 \le x \le h_1$$
$$M(x) = 0 \qquad h_1 \le x \le H$$

$$\Delta_m \cdot 1 = \frac{1}{EI}\int_0^{h_1} P_1(h_1 - x)^2\,dx$$

$$\Delta_m \cdot 1 = \frac{h_1^3 P_1}{3EI}$$

$$V(x) = P_1 \qquad 0 \le x \le h_1$$
$$V(x) = 0 \qquad h_1 \le x \le H$$

$$\Delta_v \cdot 1 = \frac{1}{E_v A}\int_0^{h_1} P_1\,dx = \frac{P_1 h_1}{E_v A}$$

Deflection at A:

$$\Delta_A = \sum_{i=1}^{10} \frac{h_i^3 P_i}{3EI} + \sum_{i=1}^{10} \frac{P_i h_i}{E_v A}$$

BASE SHEAR = $\sum_{i=1}^{10} P_i$

Cantilever Beam Calculation

General Properties		*Item Description*
f'_{m_90}	1.17 ksi	Compressive strength of brick ⊥ bed joint (ASCE 41 Table 7-1 and 7-2
E_{me_90}	900.9 ksi	Young's modulus of brick ⊥ bed joint = $700f'_{m\_90}$ (ACI 530 1.8.2.2.1)
G	360.36 ksi	Shear Modulus=$.4E_{me\_90}$ (ASCE 41 7.2.2.7)
L_{inf}	264 in	Length of infill panel
t_{inf}	12 in	Thickness of masonry infill, composite properties
I_{inf}	18399744 in	
A_{inf}	3168 in^2	

$$F_i = \frac{m_i \phi_i}{\sum_{j=1}^{n} m_j \phi_j} F_b$$

Pushover loads (kip)

Floor	Height (in)	Shape	mass	P1	P2	P3	P4	P5	P6	P7	P8	P9	P10
1	160	0.023249	0.1	0.023344	0.233437	0.350155	0.466873	0.583592	0.70031	0.817028	0.933747	1.050465	1.167183
2	416	0.272033	0.1	0.27314	2.731402	4.097103	5.462803	6.828504	8.194205	9.559906	10.92561	12.29131	13.65701
3	602	0.453634	0.1	0.45548	4.554799	6.832199	9.109599	11.387	13.6644	15.9418	18.2192	20.4966	22.774
4	788	0.620975	0.1	0.623502	6.235022	9.352534	12.47004	15.58756	18.70507	21.82258	24.94009	28.0576	31.17511
5	974	0.766237	0.1	0.769356	7.693556	11.54033	15.38711	19.23389	23.08067	26.92745	30.77422	34.621	38.46778
6	1160	0.888592	0.1	0.892209	8.922086	13.38313	17.84417	22.30522	26.76626	31.2273	35.68834	40.14939	44.61043
7	1314	0.955014	0.1	0.9589	9.589003	14.3835	19.17801	23.97251	28.76701	33.56151	38.35601	43.15051	47.94501
8	1468	1	0.1	1.00407	10.0407	15.06104	20.08139	25.10174	30.12209	35.14243	40.16278	45.18313	50.20348
	6882	Σ		5	50	75	100	125	150	175	200	225	250
		Δ_A (in)		0.163184	1.63184	2.44776	3.26368	4.0796	4.895521	5.711441	6.527361	7.343281	8.159201
		Δ/H (in./in.)		0.000103	0.00103	0.001545	0.00206	0.002576	0.003091	0.003606	0.004121	0.004636	0.005151

Appendix D
Limit State Analysis Calculations

Limit State Analysis of Bay

$M_p = F_y \cdot Z$

$F_y = 23$ ksi

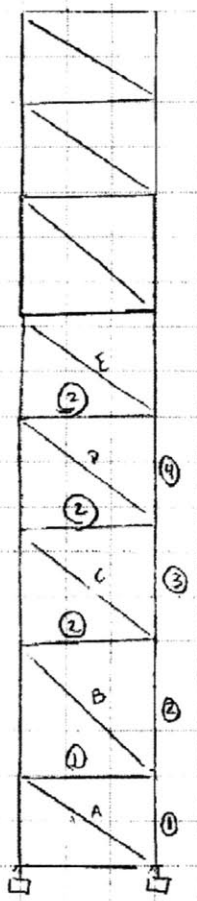

Column Properties

Col 1 = W14 x 342 $\quad Z = 672 \text{ in}^3$

$M_{pc1} = (23)(672) = 15{,}456$ kip-in

Col 2 = W14 x 311 $\quad Z = 603 \text{ in}^3$

$M_{pc2} = (23)(603) = 13{,}869$ kip-in

Col 3 = W14 x 257 $\quad Z = 487 \text{ in}^3$

$M_{pc3} = (23)(487) = 11{,}201$ kip-in

Col 4 = W14 x 211 $\quad Z = 390 \text{ in}^3$

$M_{pc3} = (23)(390) = 8970$ kip-in

Beam Properties

Beam 1 = W14 x 257 $\quad Z = 487 \text{ in}^3$

$M_{pB1} = 11{,}201$ kip-in

Beam 2 = W14 x 176 $\quad Z = 320 \text{ in}^3$

$M_{pB2} = (23)(320) = 7360$ kip-in

Strut Properties (for calculations see Appendix B)

$R_A =$ 212 kips

$R_B =$ 241 kips

$R_C =$ 214 kips

$R_D =$ 214 kips

$R_E =$ 214 kips

CONSIDER FIRST A SINGULAR BAY:

1) single frame (NO INFILL)

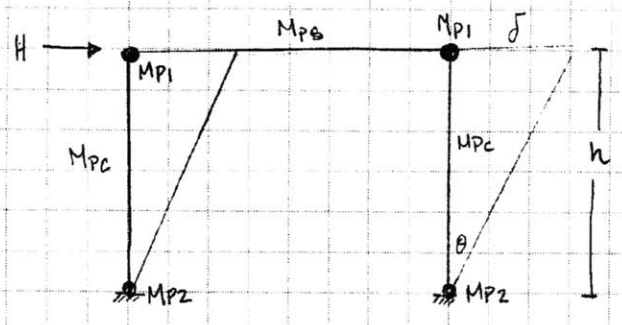

(expected failure mode)

- expected to occur for minimal gravity load and high lateral load value

M_{P1} = least of beam, column, and connection plastic resisting moment

$H\delta = (2M_{P1} + 2M_{P2})\theta$

small angles $\delta = h\theta$

$$H_{ULT} = \frac{2M_{P1} + 2M_{P2}}{h}$$

2) single frame (with infill)

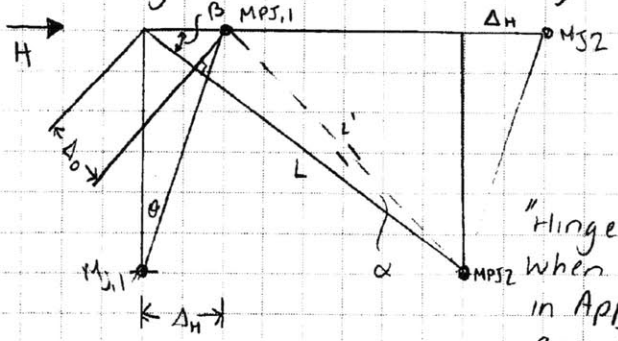

L = length of infill

L' = revised length

$\cos\alpha = \frac{L - \Delta_D}{L'}$ for small angles, $\cos\alpha \approx 1$

$L' = L - \Delta_D$

"Hinge" will form in compression strut when force exceeds allowable [calculated in Appendix B - function of f'_{me-90} and area]

Resistance contribution of infill = $R_{STRUT}\,\Delta_D$

$H\Delta_H = (M_{PJ1} + M_{PJ2} + \cancel{M_{PJ1}} + \cancel{M_{PJ2}})\theta + R_{STRUT}\,\Delta_D$

(negligible per Semenyuk)

$$H_{ULT} = \frac{(M_{PJ1} + M_{PJ2})}{H} + \frac{R_{STRUT} \cdot B}{L}$$

CONSIDER FULL BAY → UNLOADED CORNERS ARE LOADED CORNERS OF TWO OTHER PANELS IN FRAME

1) FAILURE MODE No. 1 (Second Story) COLUMN FAILURE at loaded corners

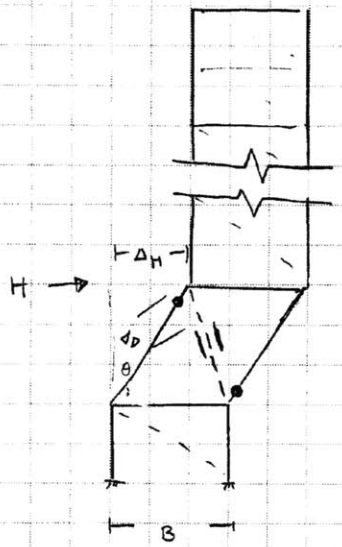

$$H\,\Delta_H = 2M_{PC2}\theta + R_{STRUT}\,\Delta_D$$

$$H = \frac{2M_{PC2}}{h} + \frac{R_{STRUT}\,B}{L}$$

$$H_{ULT} = \frac{2(13{,}869)\left(\frac{1}{12}\right)\ \text{kip-FT}}{21.33\ \text{FT}} + \frac{241\ \text{kips} \cdot 22\ \text{FT}}{\text{SQRT}\left(22^2 + 21.33^2\right)}$$

T
h 21'4"
I

$$H_{ULT} = 109 + 173$$

$$H_{ULT} = 282\ \text{KIPS}$$

2) FAILURE MODE No. 2 (SECOND STORY) corner crushing beam failure

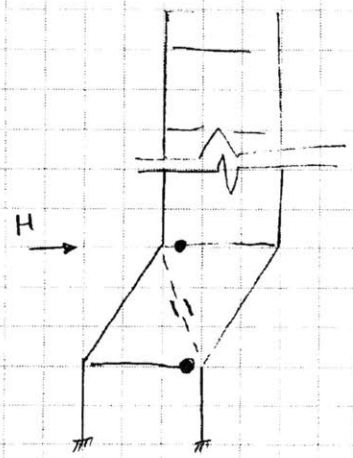

$$H_{ULT} = \frac{2M_{PC1}}{h} + \frac{R_{STRUT}\,B}{L}$$

$$H_{ULT} = \frac{2(7360)\left(\frac{1}{12}\right)}{21.33} + 173$$

$$H_{ULT} = 230\ \text{KIPS}$$

[SAP 2000 PREDICTED 240 kip collapse limit] COLUMN FAIL = upper limit.

FULL ELEVATION (9 bays)

20 HINGES

a) column failure

$$H_{ULT} = \frac{18}{21.33}\left(\frac{13869}{12}\right) + 9(173) = 2{,}530\ \text{KIPS}$$

[SAP 2000 predicted 1950 kip collapse